Figures

Chapter 3

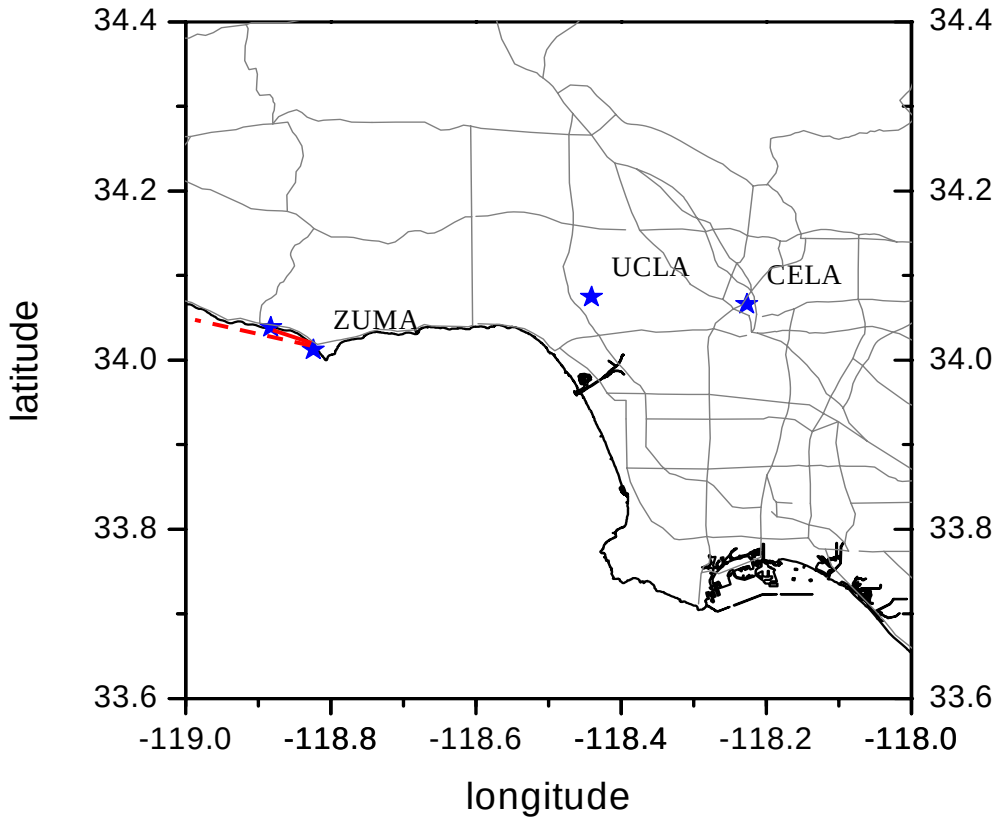

Figure 3.0.1. Map of field site locations for the Zuma Beach halogen experiment. The LP DOAS light path is indicated by the red line. Unmarked star at the west end of the LP DOAS light path indicates El Matador State Beach – location of the LP DOAS retro reflector array. The MAX-DOAS line of sight is shown by the red dashed line.

Figure 3.0.2. Photograph of mobile containers at the main site at Zuma Beach.

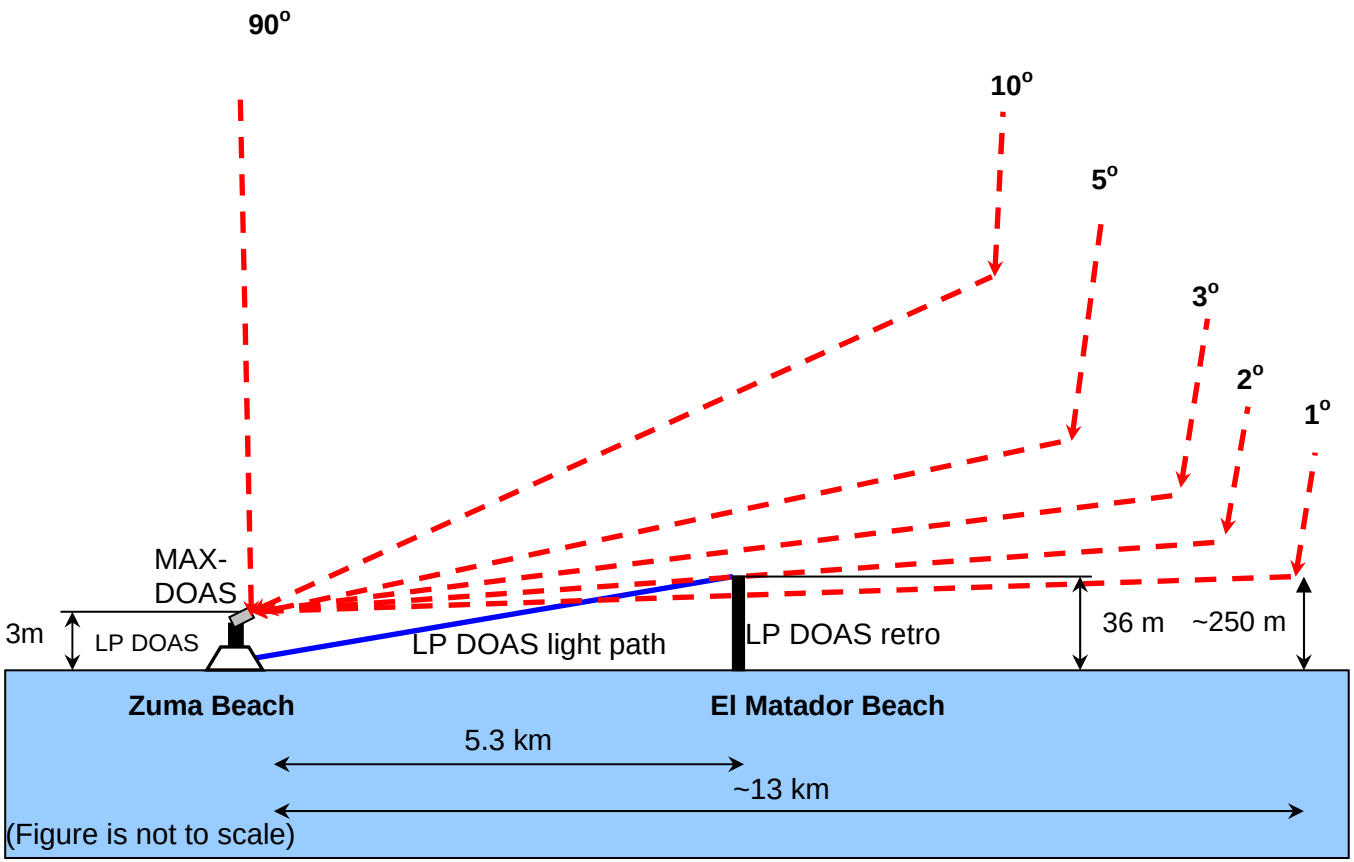

Figure 3.1.1. Schematics of the DOAS experimental set-up at Zuma Beach.

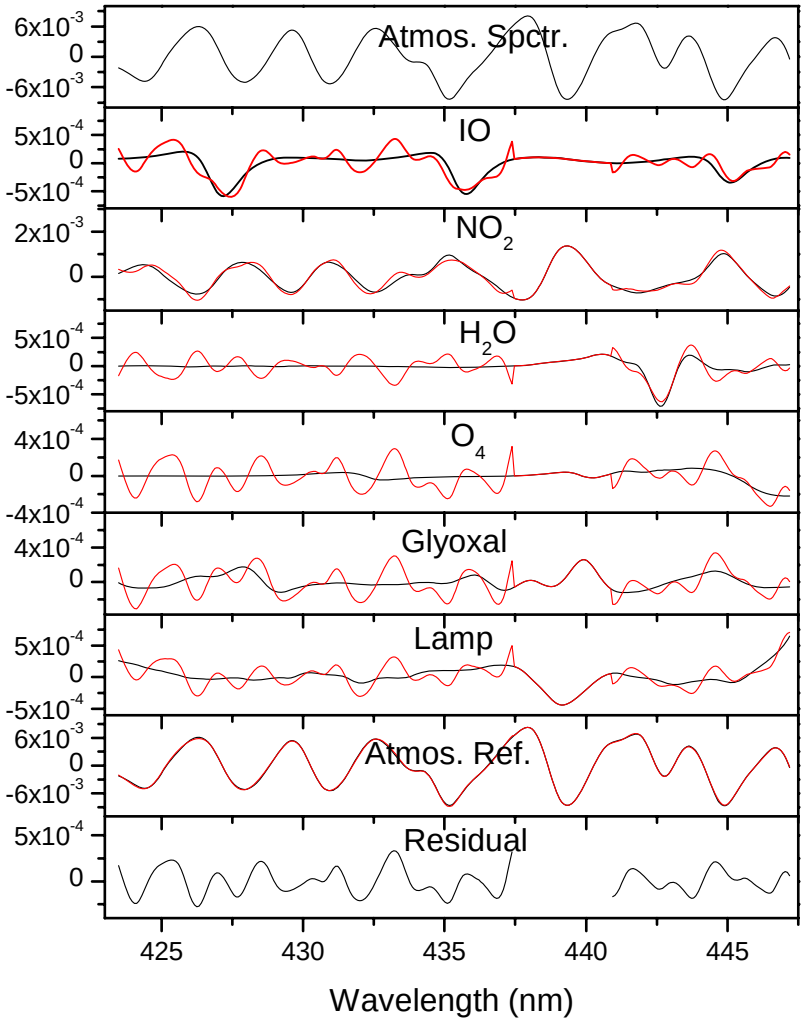

Figure 3.1.2. Example of the spectral analysis of daytime IO from the LP DOAS spectrum recorded on 10/12/2006 at 16:14 UT. The red lines represent the spectral references. The black lines represent fit results, i.e. the fitted reference + the residual. From top to bottom of the figure the following references are shown: the atmospheric absorption spectrum, the IO, NO_2, H_2O, O_4, and Glyoxal absorptions, lamp spectrum, daytime atmospheric reference spectrum, and residual. The region from 437 to 441 nm was excluded from the analysis due to spectral interferences, most likely caused by the instrument. The absorption structure of IO was clearly identified in this spectrum. The IO mixing ratio was determined to be 2.0 +/- 0.3 ppt.

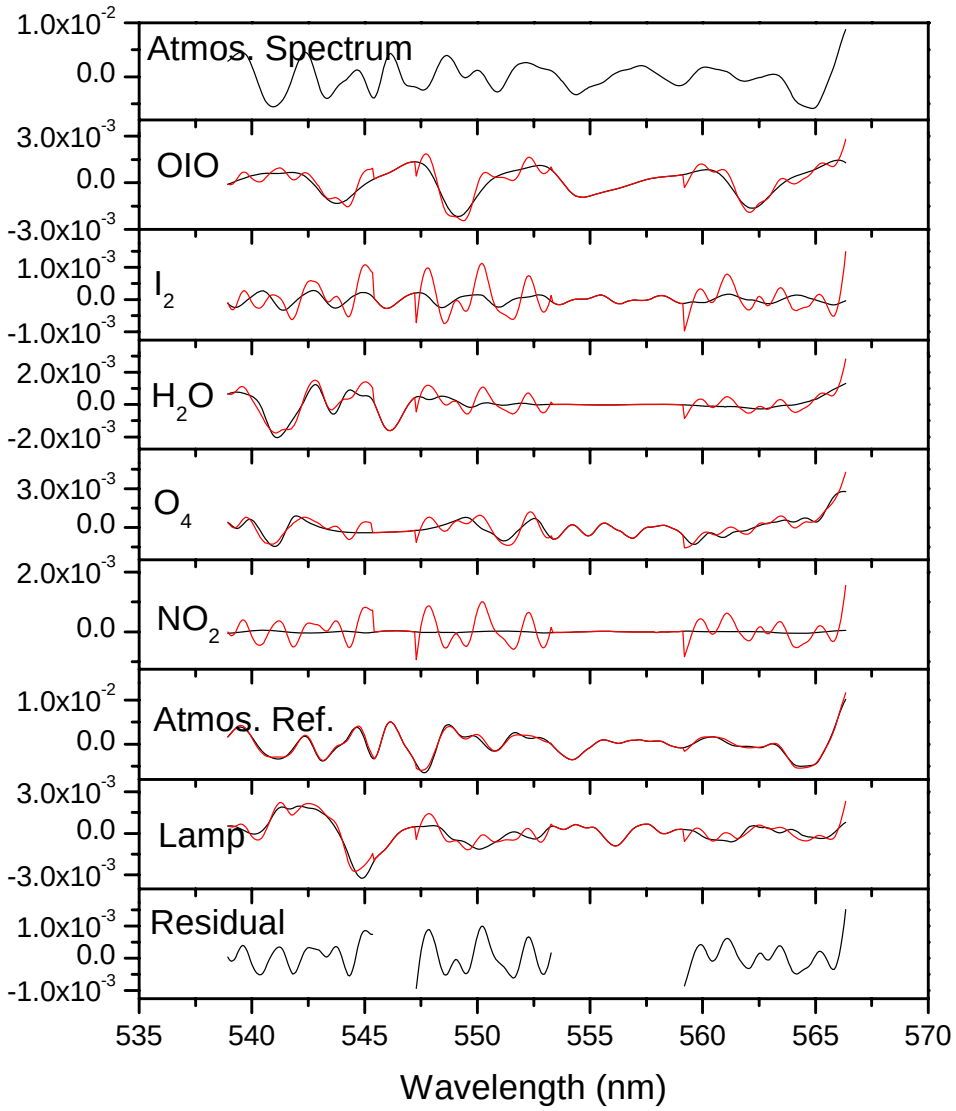

Figure 3.1.3. Example of the spectral analysis of daytime OIO from the LP DOAS spectrum recorded on 10/13/2006 at 13:06 UT. The black lines represent the spectral references. The red lines represent fit results, i.e. the fitted reference + the residual. From top to bottom of the figure the following references are shown: the atmospheric absorption spectrum, the OIO, I_2, H_2O, O_4, and NO_2 absorptions, atmospheric reference spectrum, lamp spectrum, and residual. The regions from 546 to 547.5 nm and 553 to 559 were excluded from the analysis due to spectral interferences, most likely caused by the instrument. The absorption structure of IO was clearly identified in this spectrum. The OIO mixing ratio was determined to be 23.5 ± 2.2 ppt.

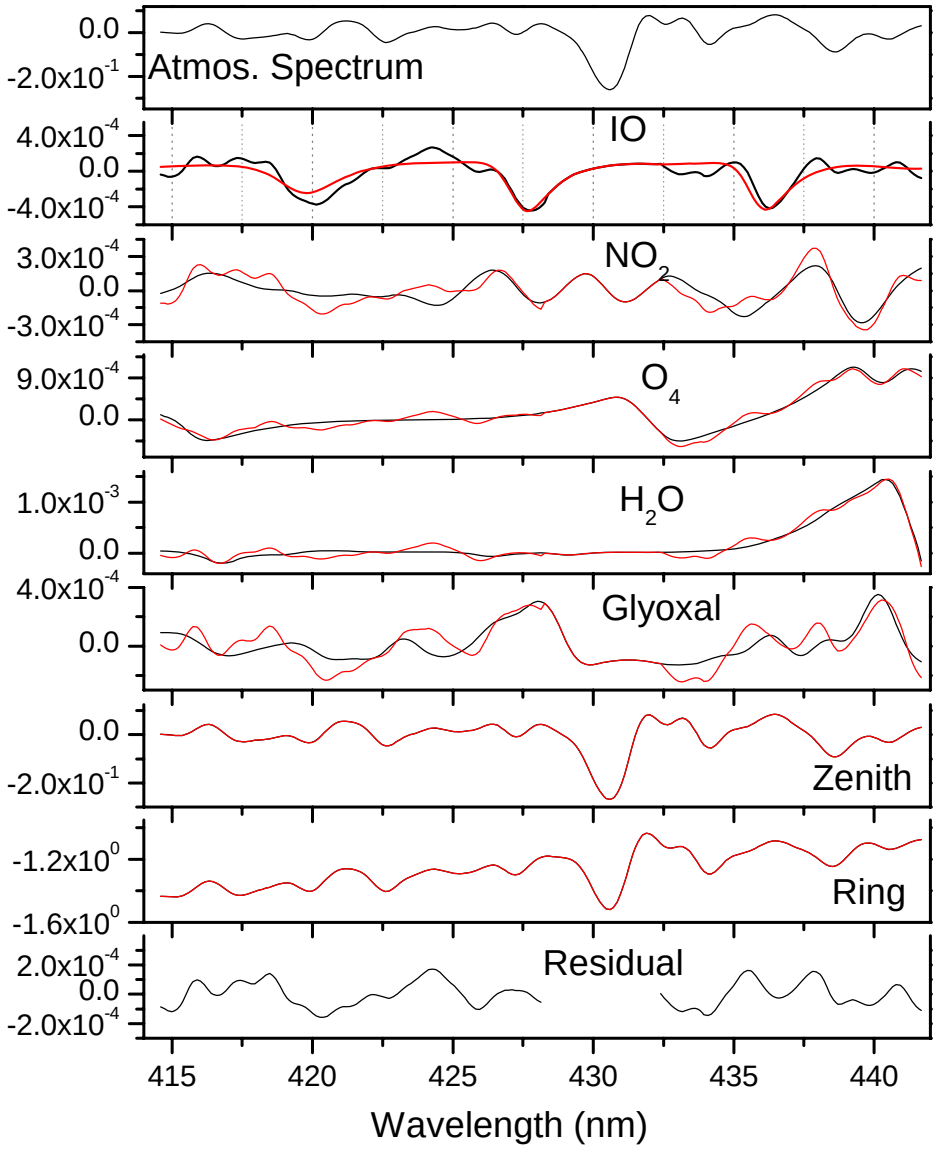

Figure 3.1.4. Example of the spectral analysis of daytime IO from the 1° elevation viewing angle MAX-DOAS spectrum recorded on 10/11/2006 at 19:26 UT. Red lines represent the spectral references. Black lines represent fit results, i.e. the fitted reference + the residual. The region from 428 to 432 nm was excluded from the analysis due to spectral interferences from either unknown absorbers or the instrument. The IO DSCD was found to be (4.09 +/- 0.22) x 10^{13} molec/cm^2.

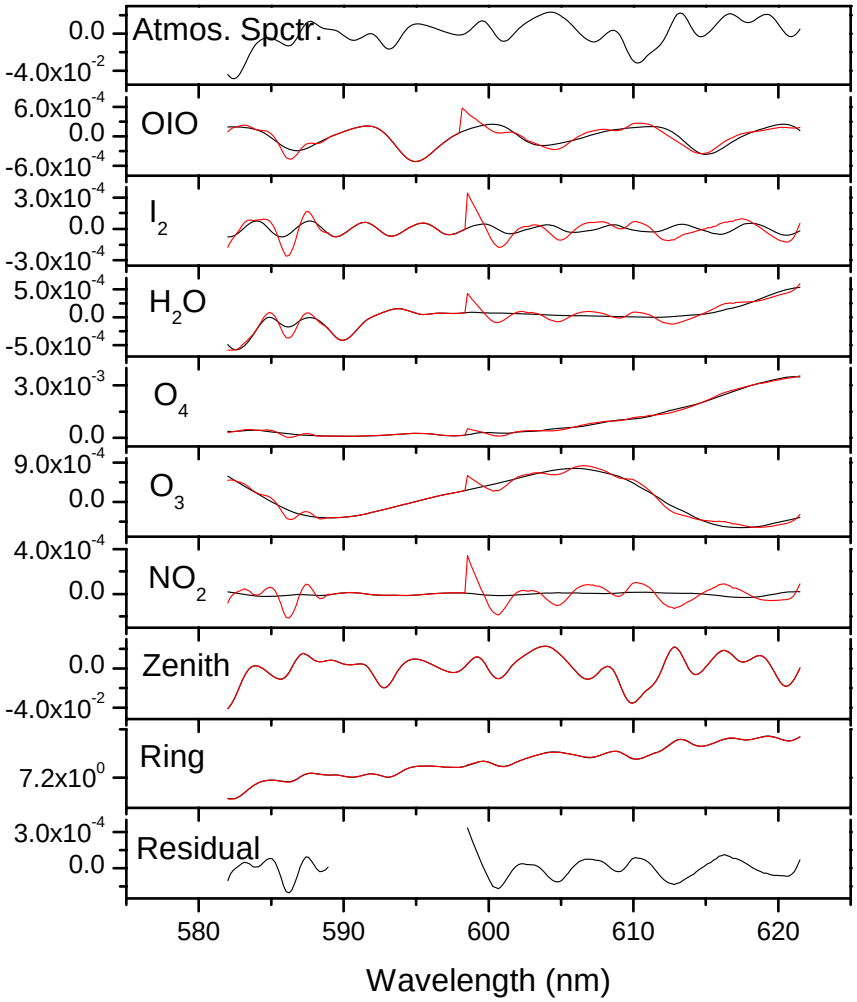

Figure 3.1.5. Example of the spectral analysis of daytime OIO from the 1° elevation viewing angle MAX-DOAS spectrum recorded on 10/18/2006 at 19:34 UT. Black lines represent the spectral references. Red lines represent fit results, i.e. the fitted reference + the residual. The region from 590 to 597 nm was excluded from the analysis due to spectra interferences from either unknown absorbers or the instrument. The OIO DSCD was found to be (1.2 ± 0.11) x 10^{14} molec/cm^{2}.

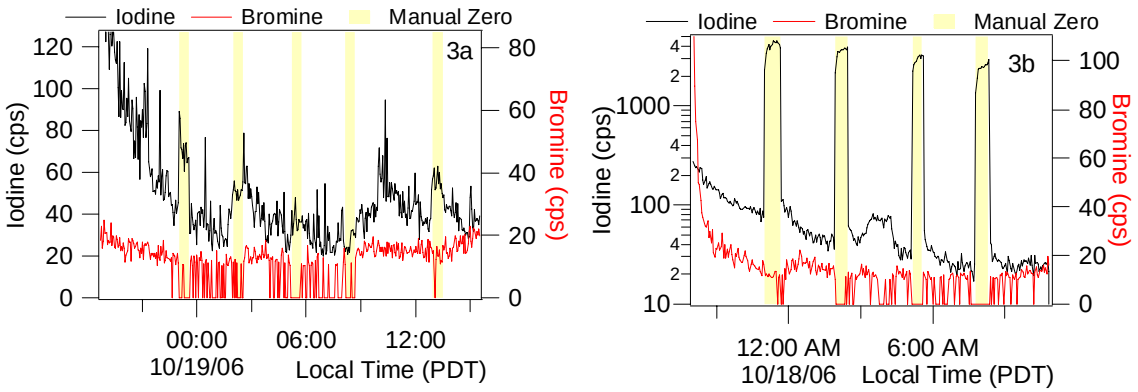

Figure 3.2.1. Impact of denuder placement and composition on I_2 and Br_2 response, shown in counts per second (cps). Data in the left panel were obtained using a denuder coated only with sodium carbonate that was positioned upstream of a 0.8 m ambient air inlet. Data in the right panel were obtained using a denuder coated with sodium carbonate and glycerol that was positioned downstream of a 2.8 m ambient inlet.

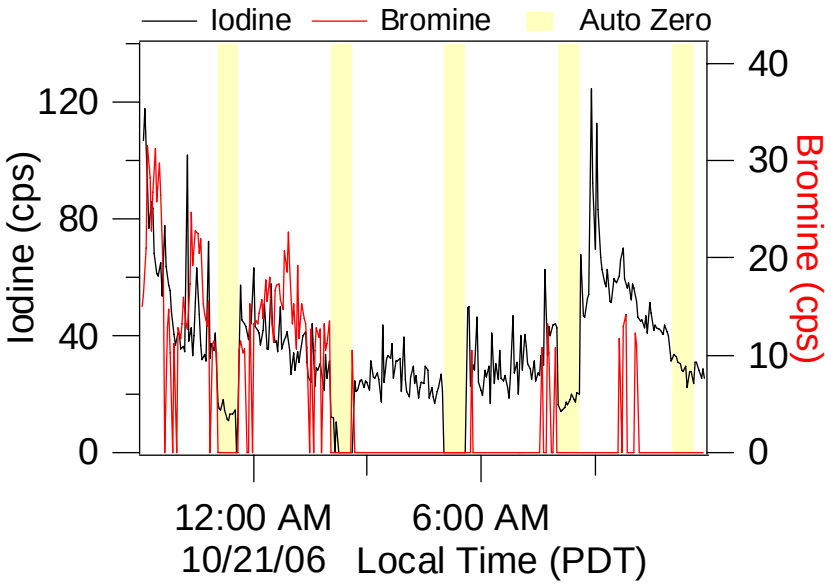

Figure 3.2.2. Iodine and bromine blanks obtained by flooding the ambient inlet with zero air.

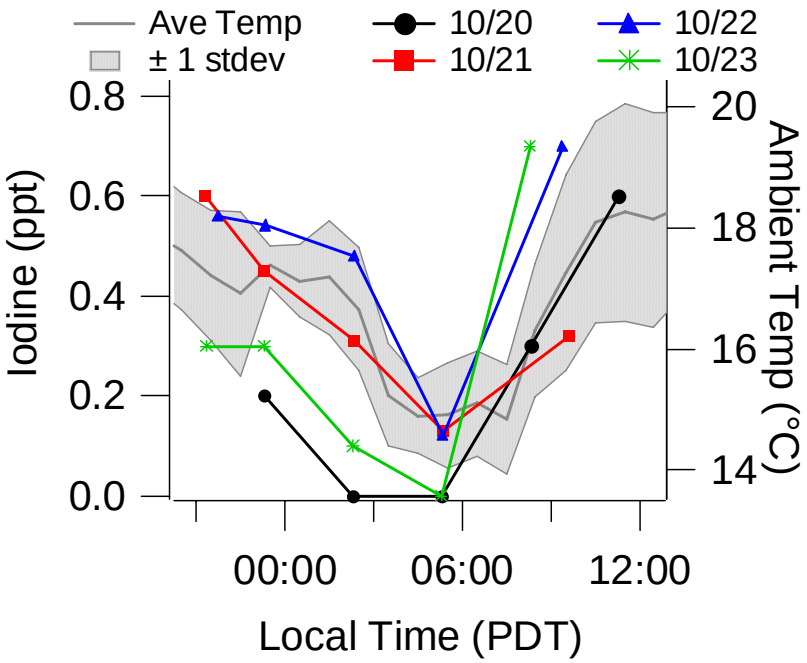

Figure 3.2.3. Automated zero air blanks for iodine plotted as a function of time of day with the average ambient temperature (Oct. 20-23).

Chapter 4

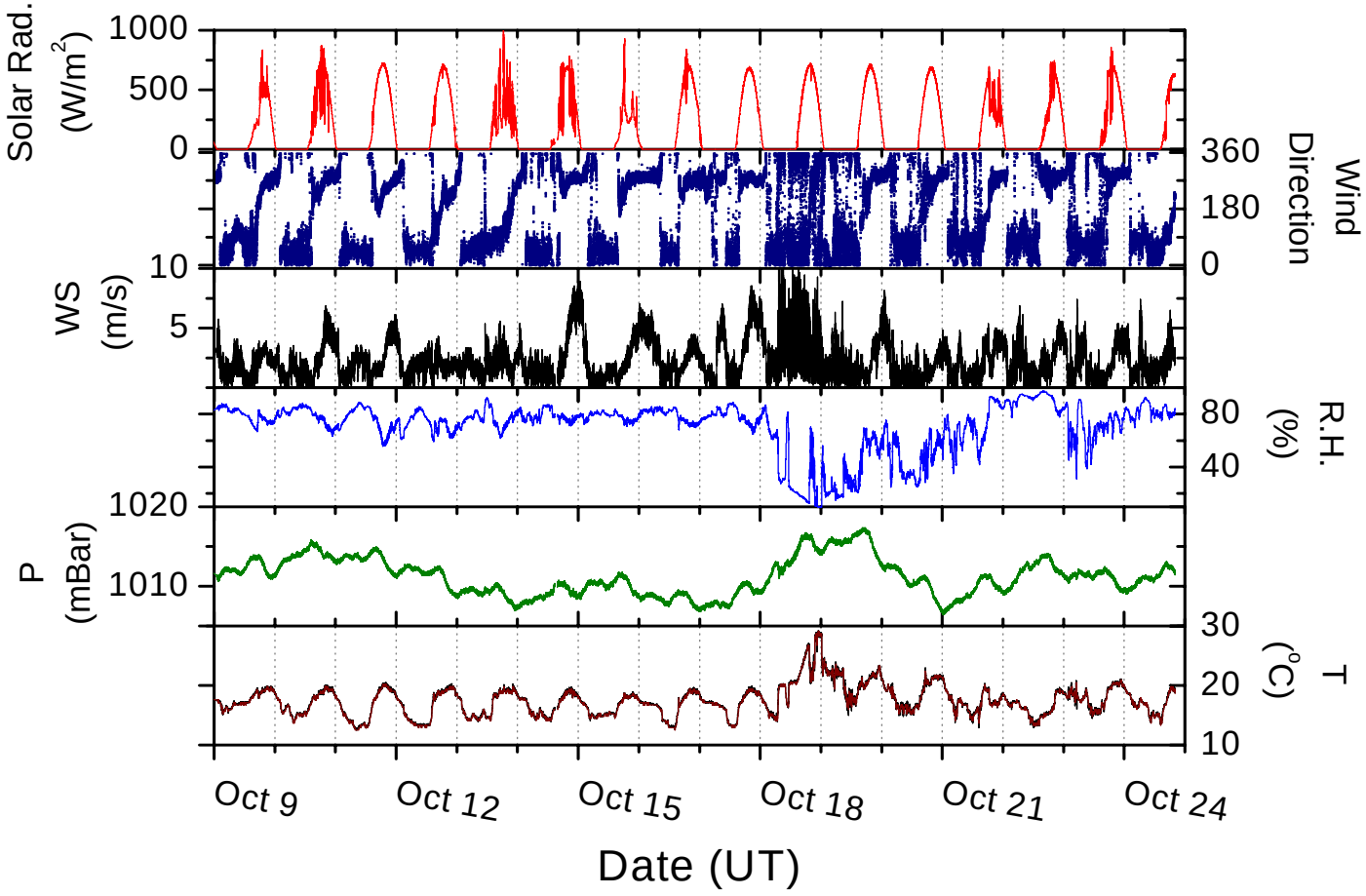

Figure 4.1.1. Meteorological data at Zuma Beach.

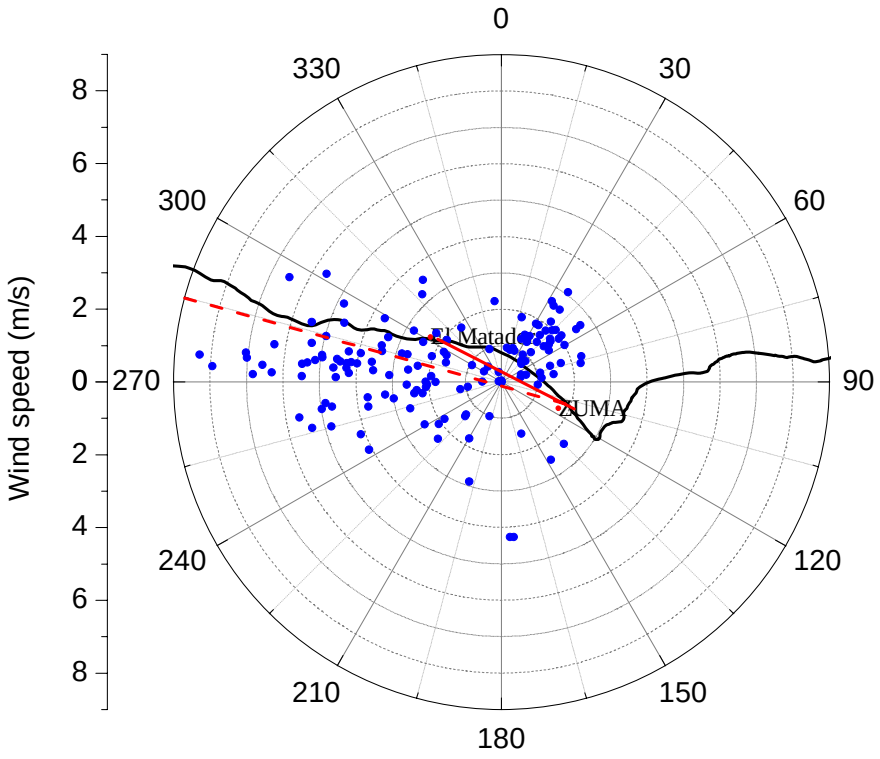

Figure 4.1.2. Daytime measurements of wind speed and wind direction for each LP-DOAS measurement during the CalHal experiment. Wind data were collected by the meteorological station located at the Zuma Beach measurement site. However, DOAS observations are representative of the measurements of concentrations averaged over the LP DOAS light path between the Zuma and El Matador beaches. We assume that wind speed and wind directions variations are negligible along the LP DOAS light path hence placing the center of the wind rose at the center of the LP DOAS light path. The locations of the LP-DOAS light path is indicated by the red solid line, while the viewing direction of the MAX-DOAS is shown as the red dashed line (see also figure 3.1).

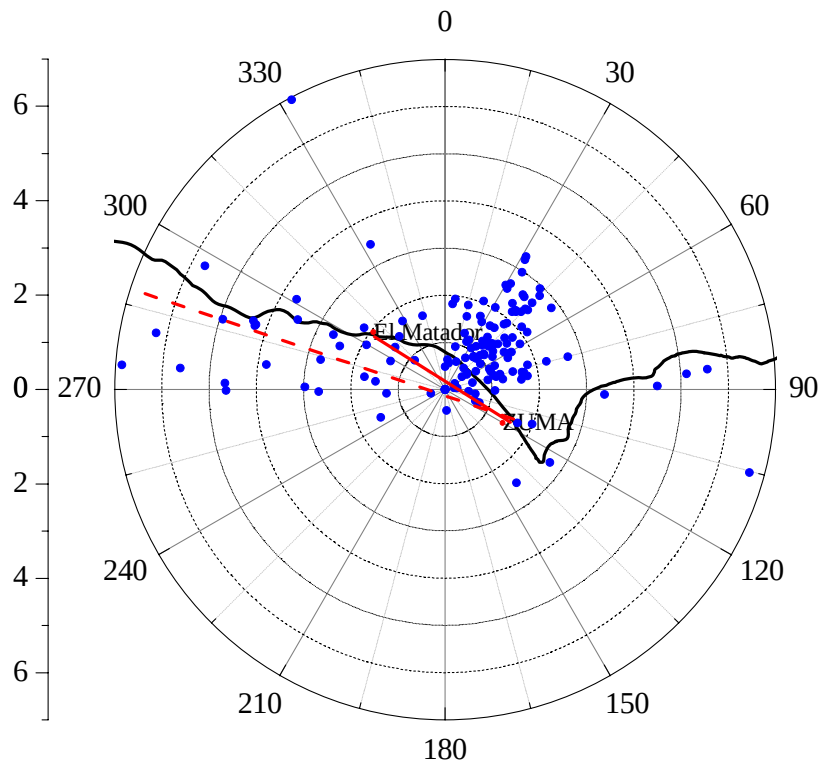

Figure 4.1.3. Nighttime measurements of wind speed and wind direction for each LP-DOAS measurement during the CalHal experiment. Wind data were collected by the meteorological station located at the Zuma Beach measurement site. However, DOAS observations are representative of the measurements of concentrations averaged over the LP DOAS light path between the Zuma and El Matador beaches. We assume that wind speed and wind directions variations are negligible along the LP DOAS light path hence placing the center of the wind rose at the center of the LP DOAS light path. The locations of the LP-DOAS light path is indicated by the red solid line, while the viewing direction of the MAX-DOAS is shown as the red dashed line (see also figure 3.1).

.

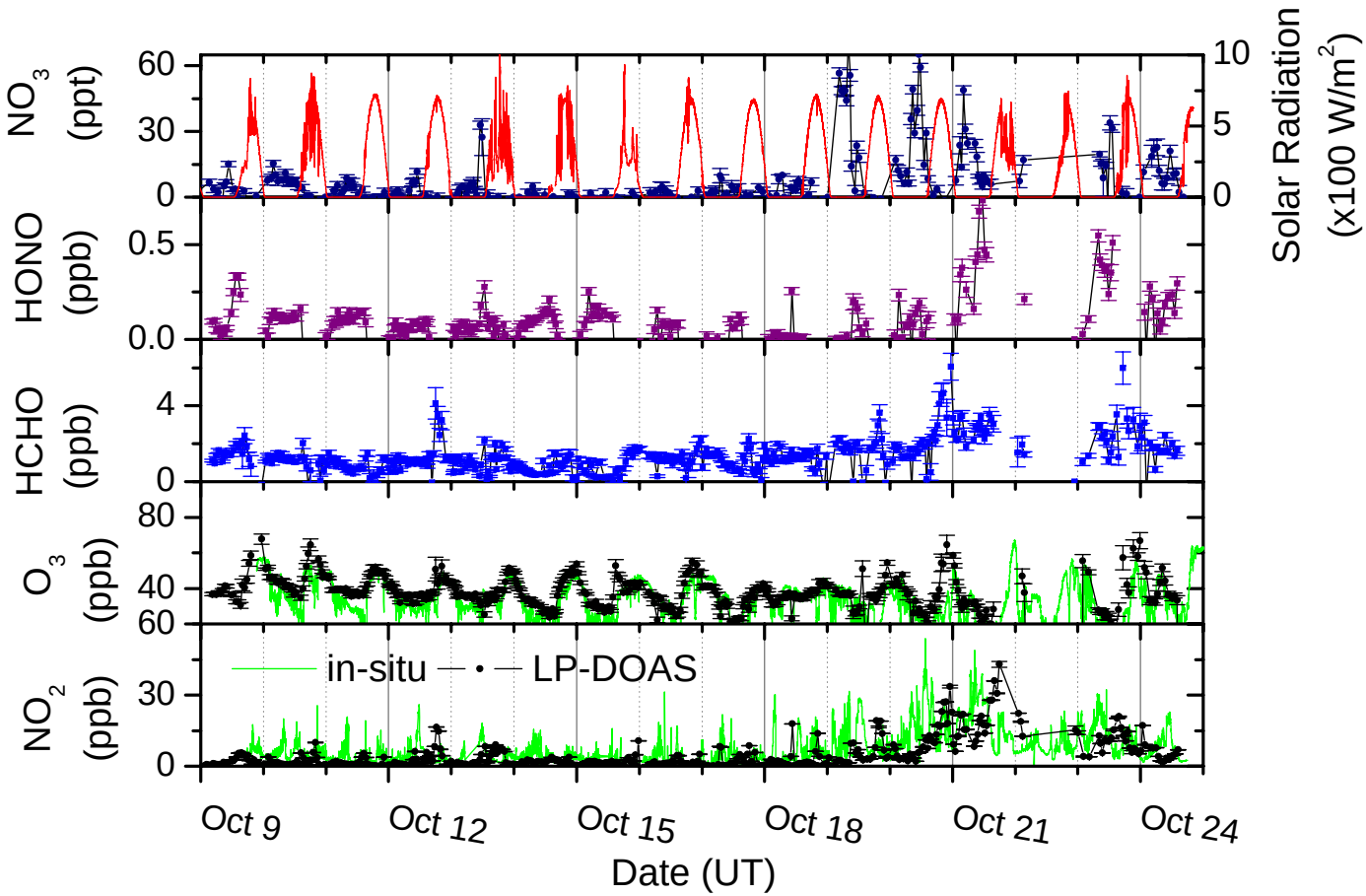

Figure 4.2.1. UCLA LP DOAS and UCI in-situ observations of pollutants at Zuma Beach. Solar radiation data is added to the top panel to orient between day and night.

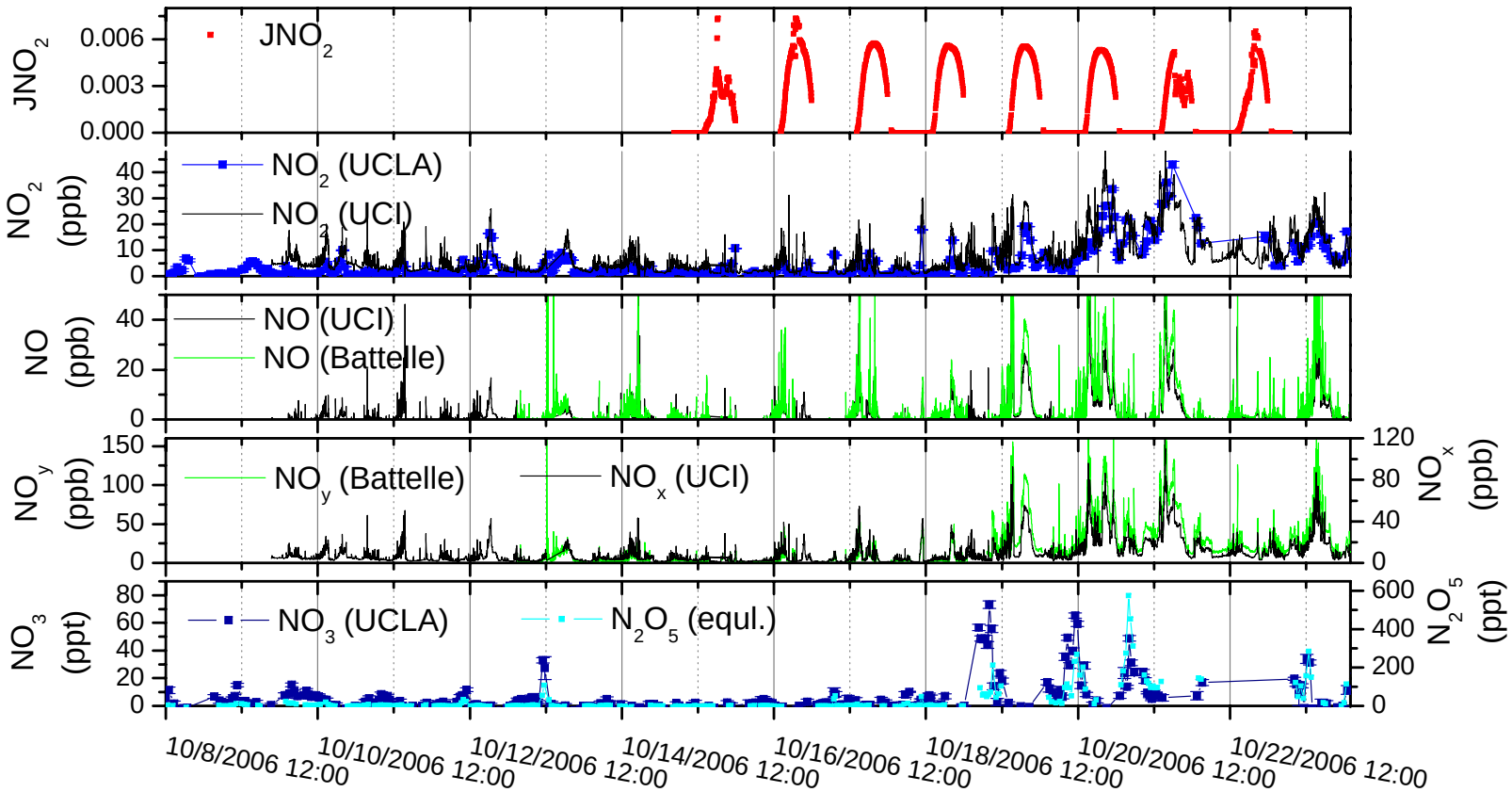

Figure 4.2.2 Observations of various nitrogen oxide species, NO_y, and the photolysis frequencies of NO_2.

.

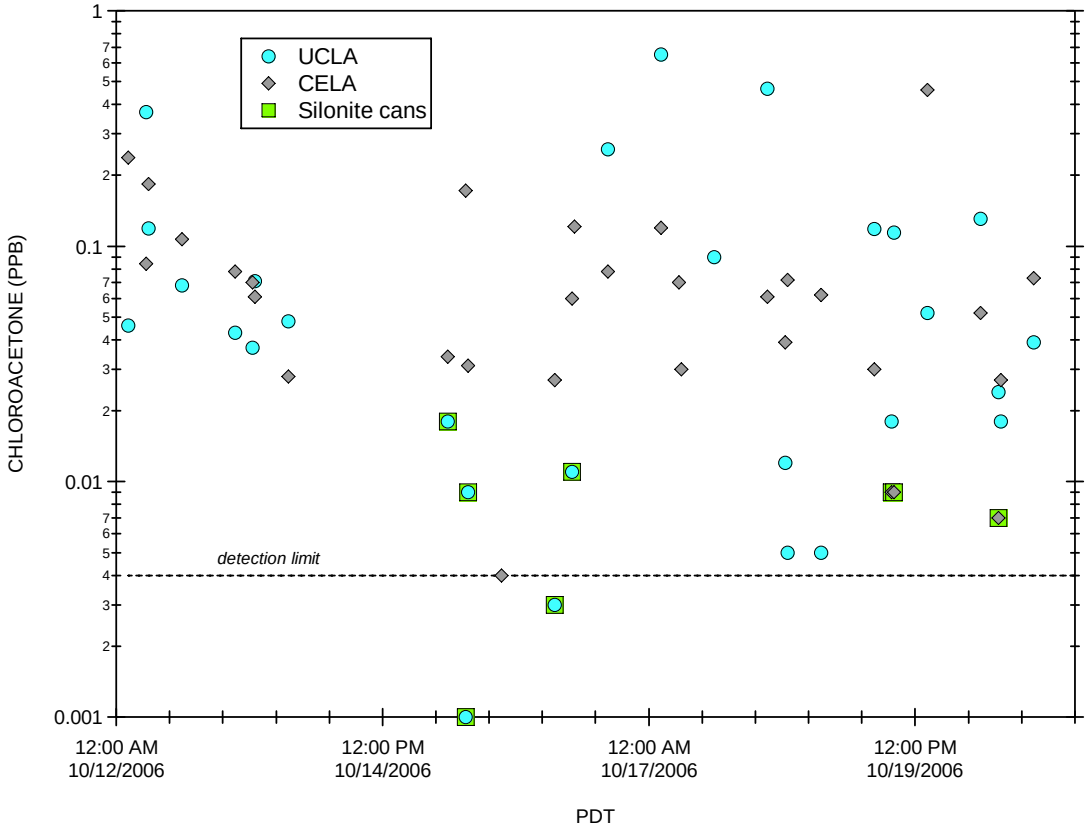

Figure 4.3.1. Chloroacetone mixing ratios initially measured in canister samples collected at the UCLA (circles) and CELA (diamonds) sites. The 4 ppt detection limit for chloroacetone is given as the dashed line. Symbols highlighted with squares are samples collected into Silonite treated canisters (Entech Inc.). Six out of a total of 12 Silonite canisters contained chloroacetone above the detection limit. (Two samples were collected only 30 minutes apart and overlap in the figure.)

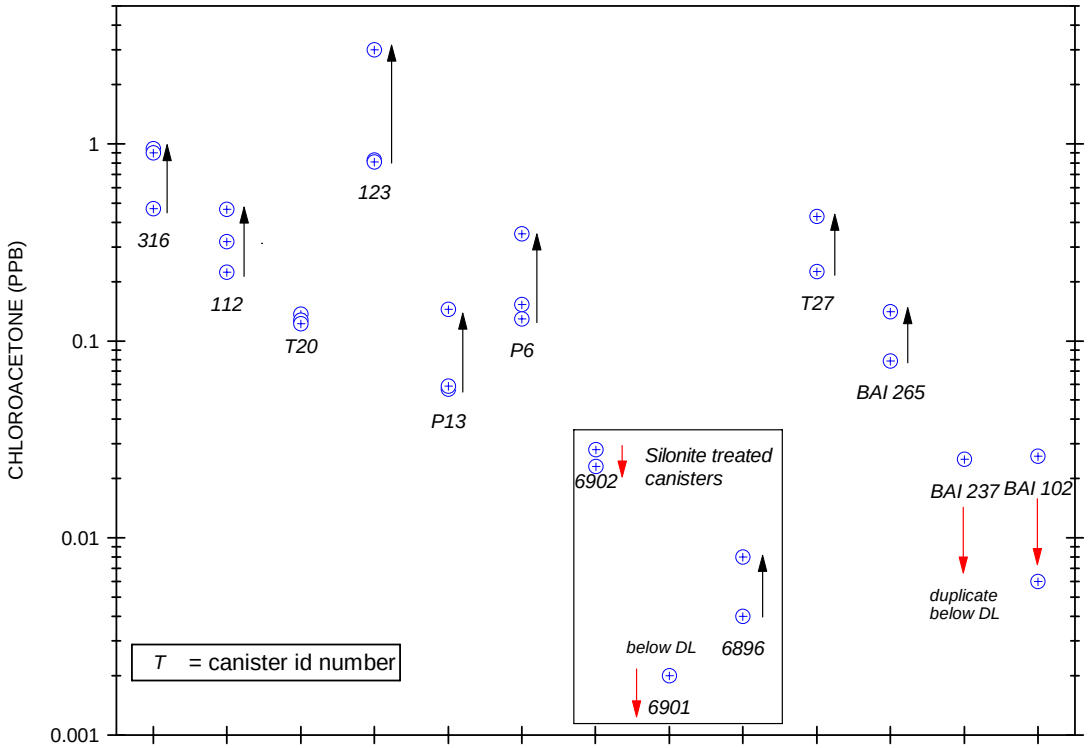

Figure 4.3.2. Replicate sample analysis results for chloroacetone. Thirteen canister samples were analyzed in duplicate or triplicate. Chloroacetone increased in most canisters with storage time (up arrows) but decreased in some canisters (down arrows).

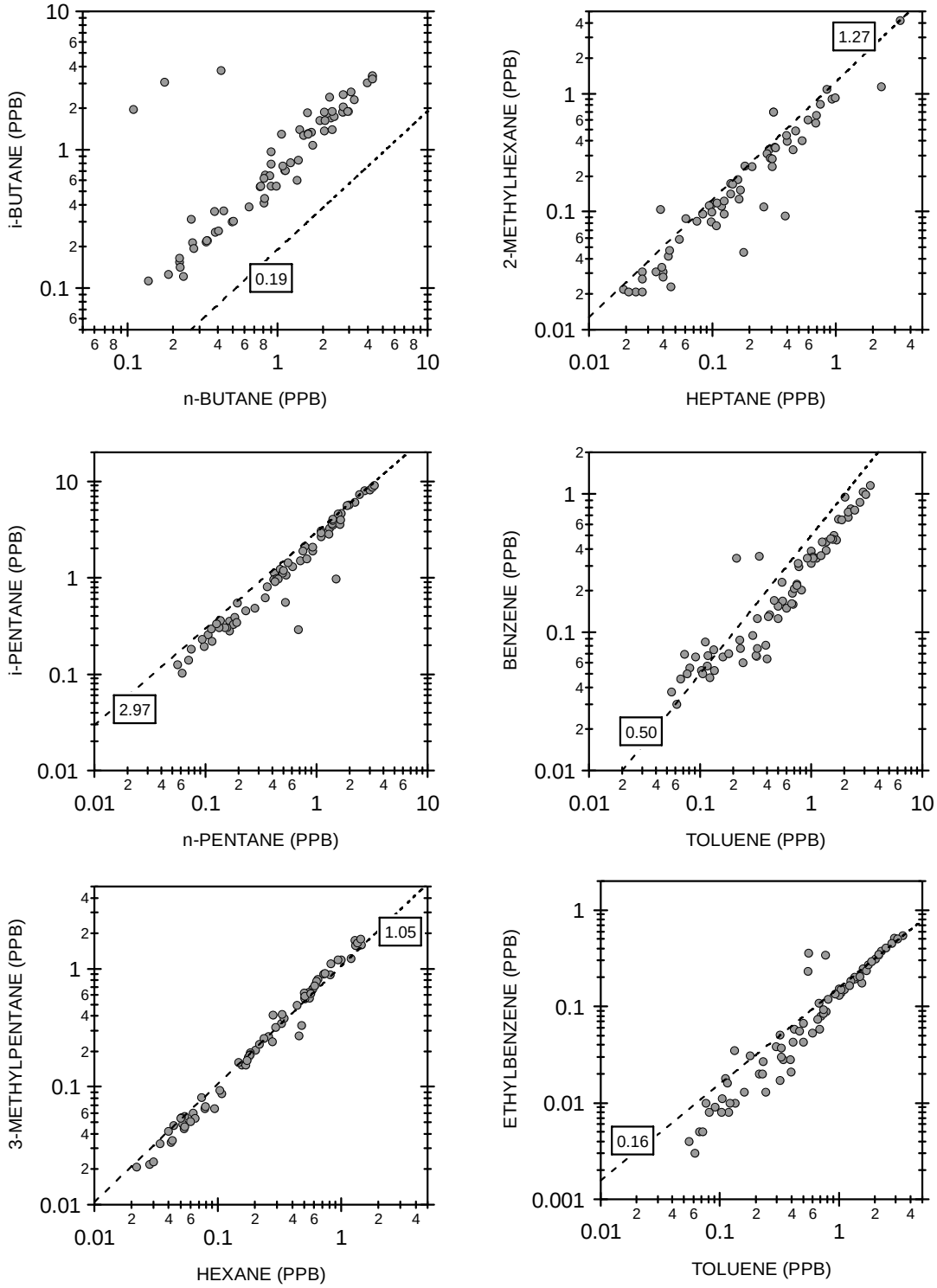

Figure 4.3.3. Correlations between hydrocarbon groups from Table 4.3 illustrating the generally good agreement of the canister data with the auto exhaust ratio shown as the dashed line. With the exception of benzene vs. toluene, the plotted pairs have very similar OH reaction rate coefficients but significantly different Cl atom rate coefficients.

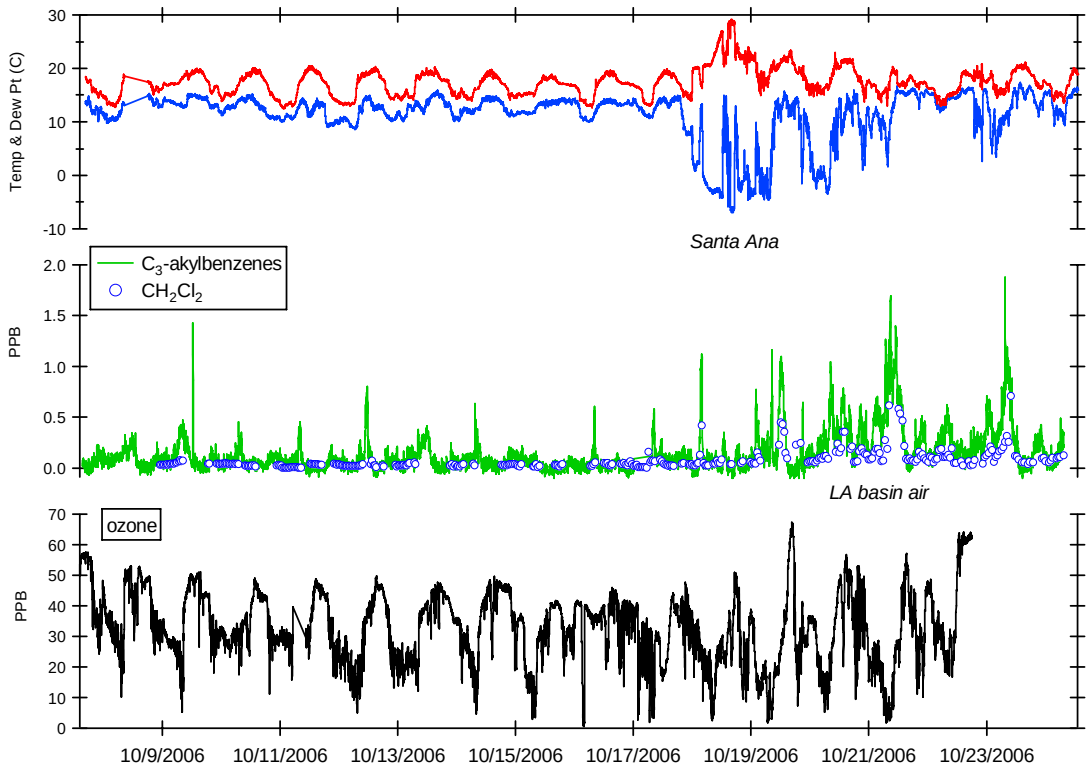

Figure 4.3.4. Hydrocarbon mixing ratios measured at Zuma Beach. Middle plot shows sum of C_3-alkylbenzene isomers as measured by the PTR-MS and CH_2Cl_2 mixing ratios as measured by GC-MS. Upper panel shows temperature (red) and dew point (blue) and bottom panel O_3 mixing ratios.

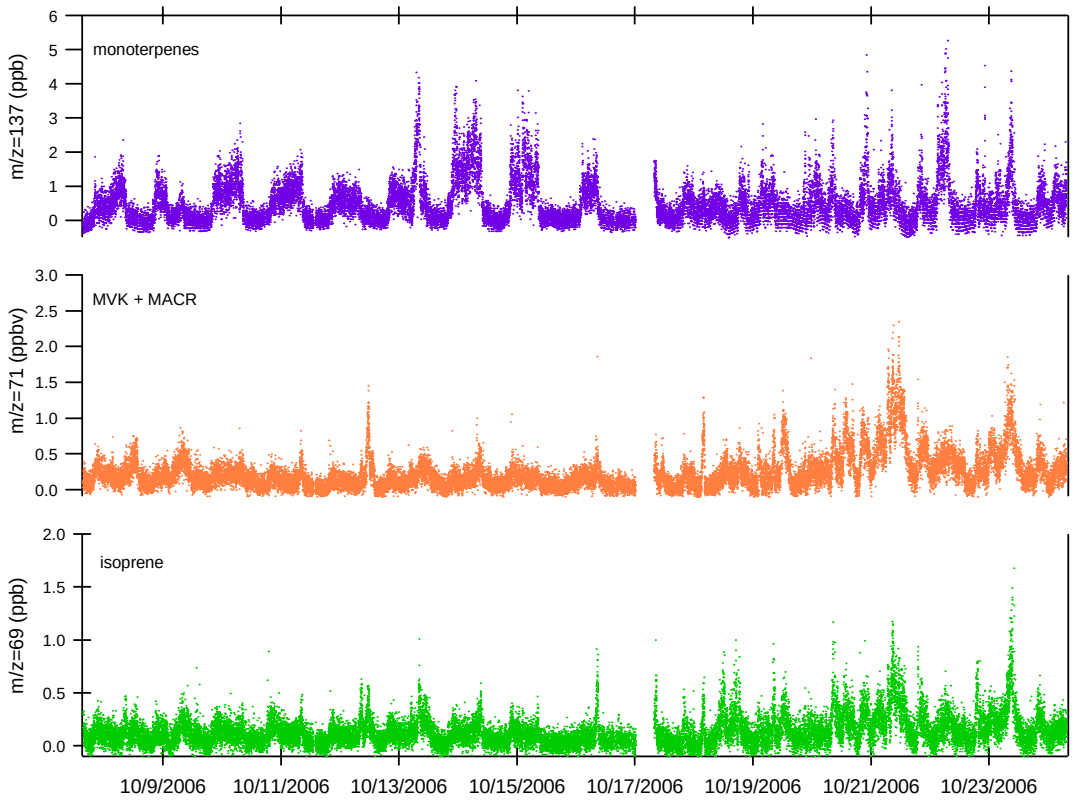

Figure 4.3.5. Zuma Beach time series isoprene, the sum of MACR and MVK, and monoterpene isomers as measured by the PTR-MS instrument.

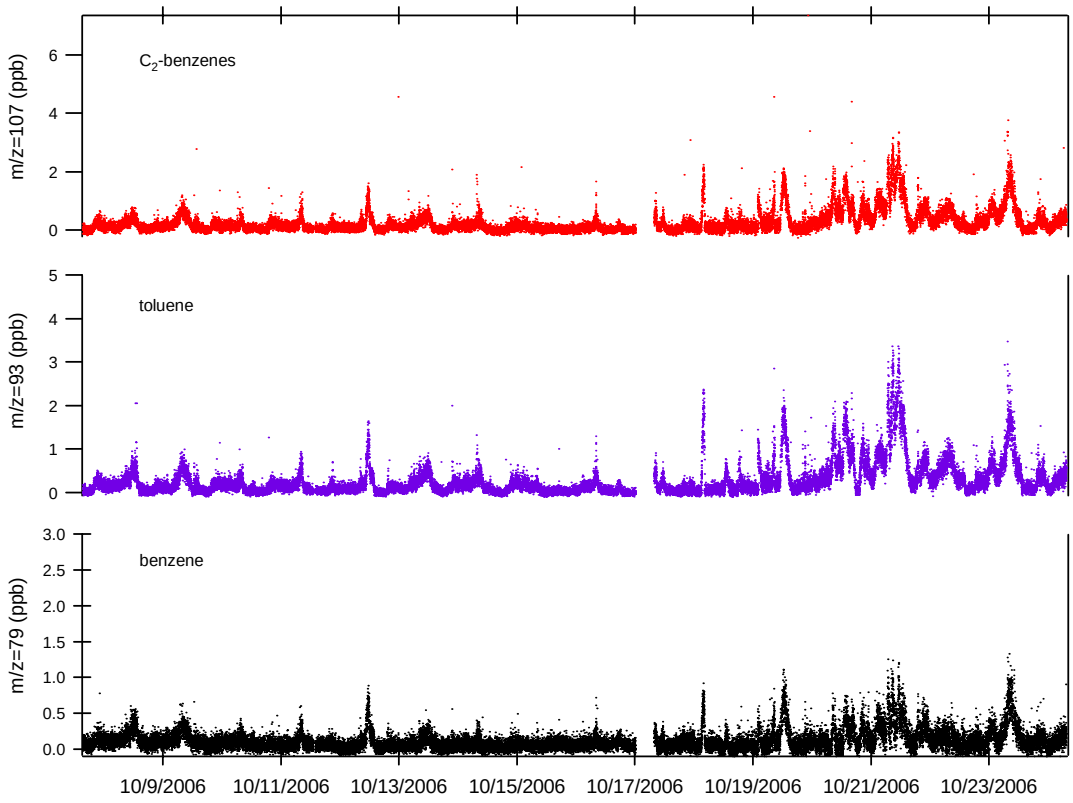

Figure 4.3.6. Zuma Beach time series of benzene, toluene, and the sum of C_2-alkylbenzene isomers as measured by the PTR-MS instrument.

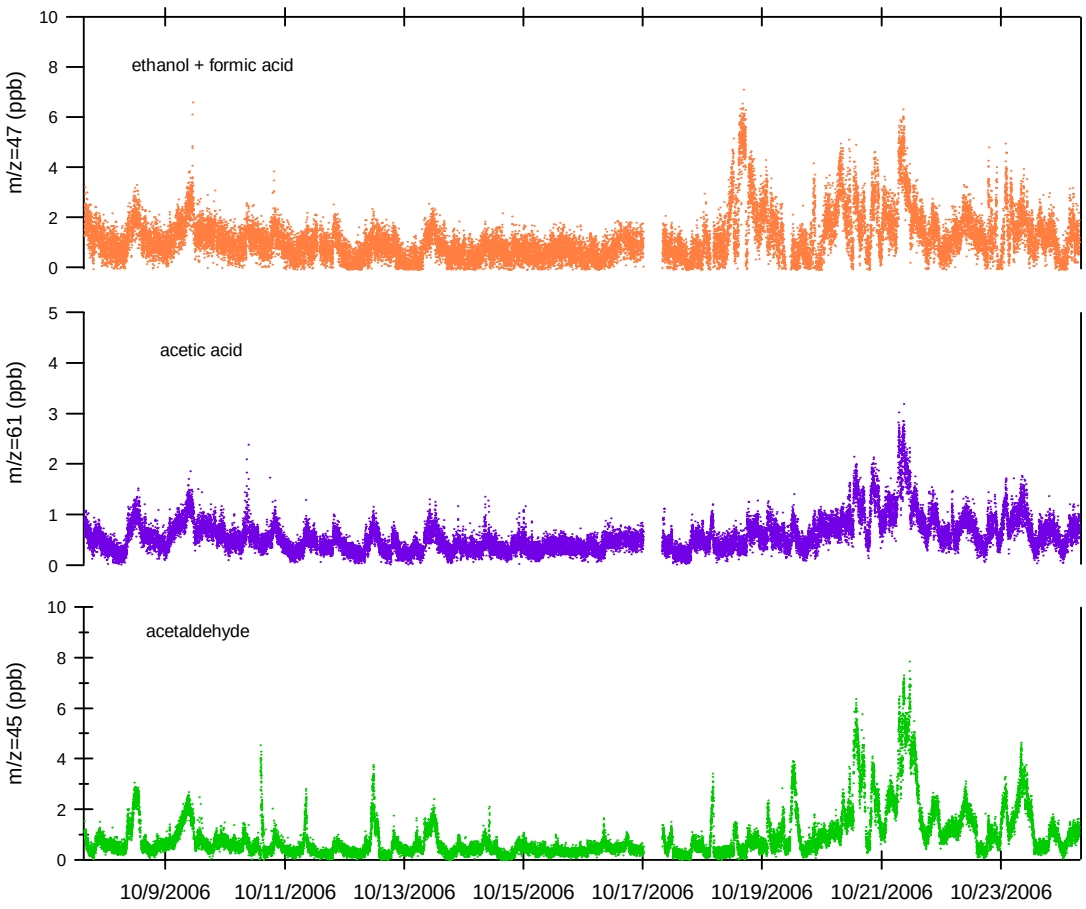

Figure 4.3.7. Zuma Beach time series of acetaldehyde, m/z=61 assumed to be acetic acid, and m/z=47 attributed to ethanol and formic acid.

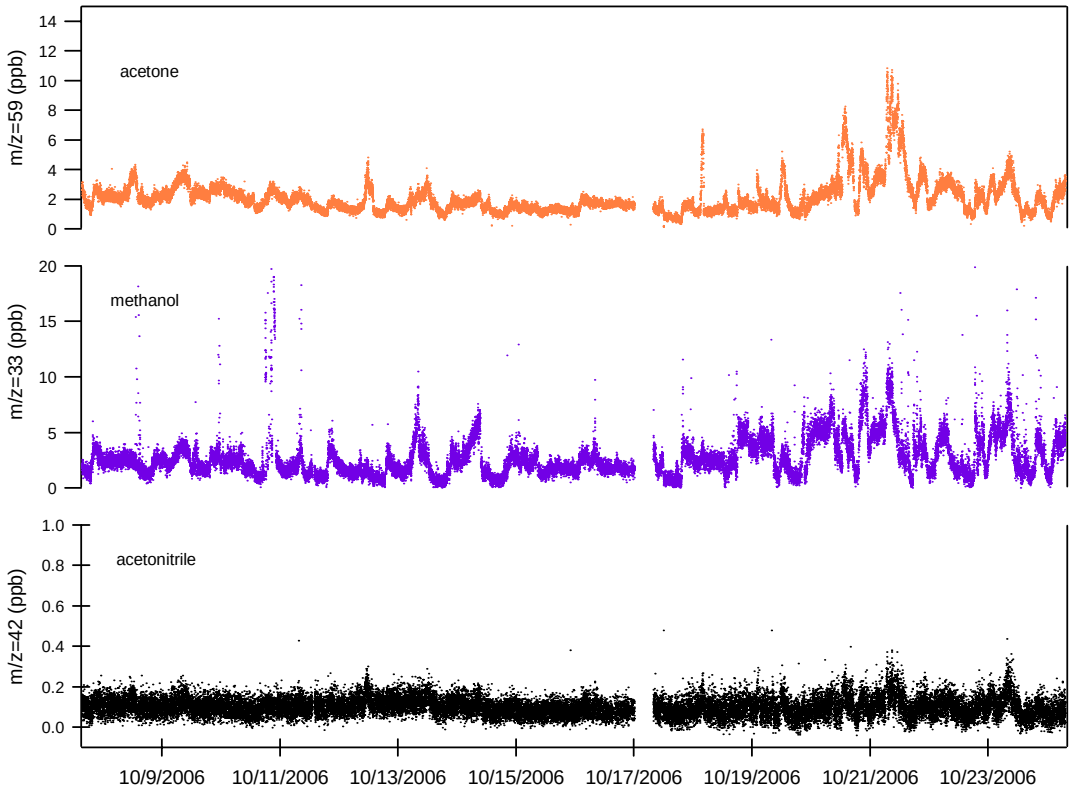

Figure 4.3.8. Zuma Beach time series of acetonitrile, methanol, and acetone as measured by the PTR-MS instrument.

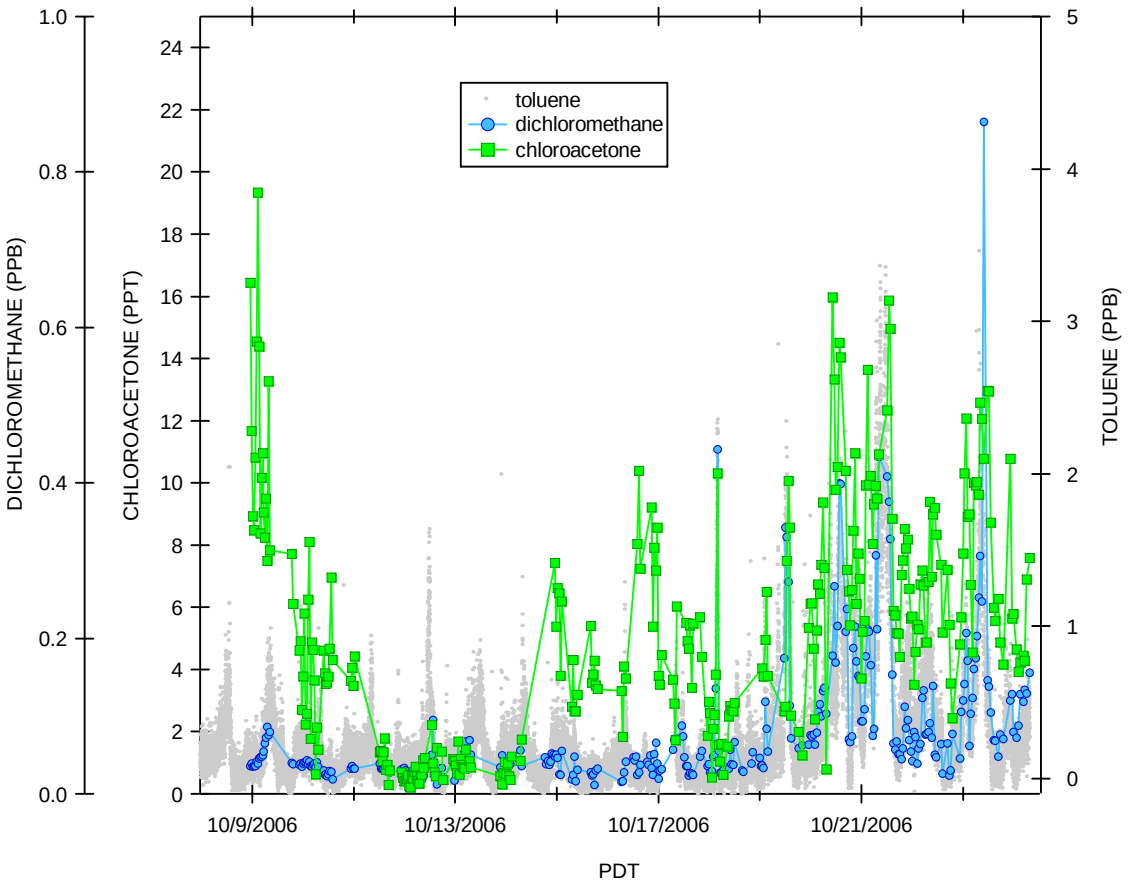

Figure 4.3.9. Zuma Beach time series of chloroacetone and CH_2Cl_2 mixing ratios measured by in-situ GC-MS and toluene mixing ratios measured by PTR-MS. Chloroacetone was significantly above the 4 ppt detection limit during three periods: clean air period from Oct 9 to Oct 10, clean air period from October 16 to October 18, and during a polluted period of LA basin outflow from October 19 to October 24.

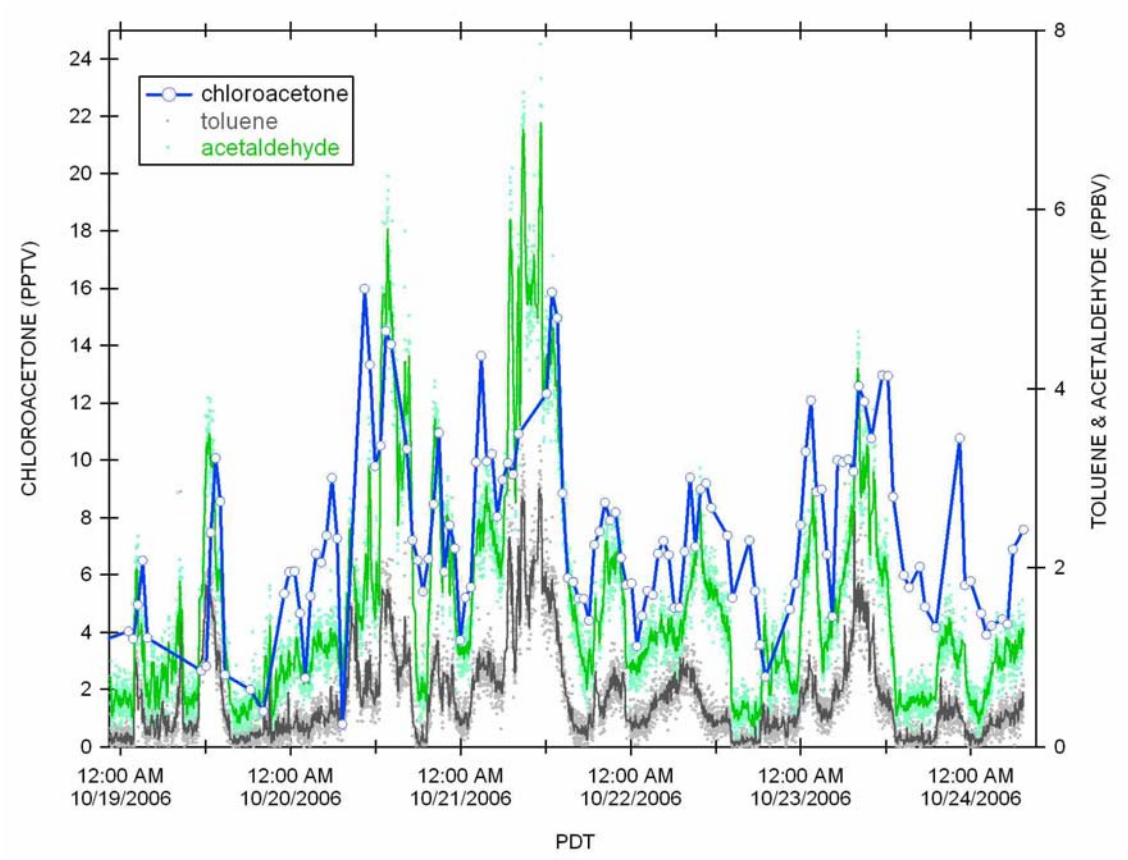

Figure 4.3.10. Time series of the October 19 to October 24 LA basin outflow period showing chloroacetone, toluene, and acetaldehyde mixing ratios. Lines through toluene and acetaldehyde data points are 11-point box smooth averages of the data.

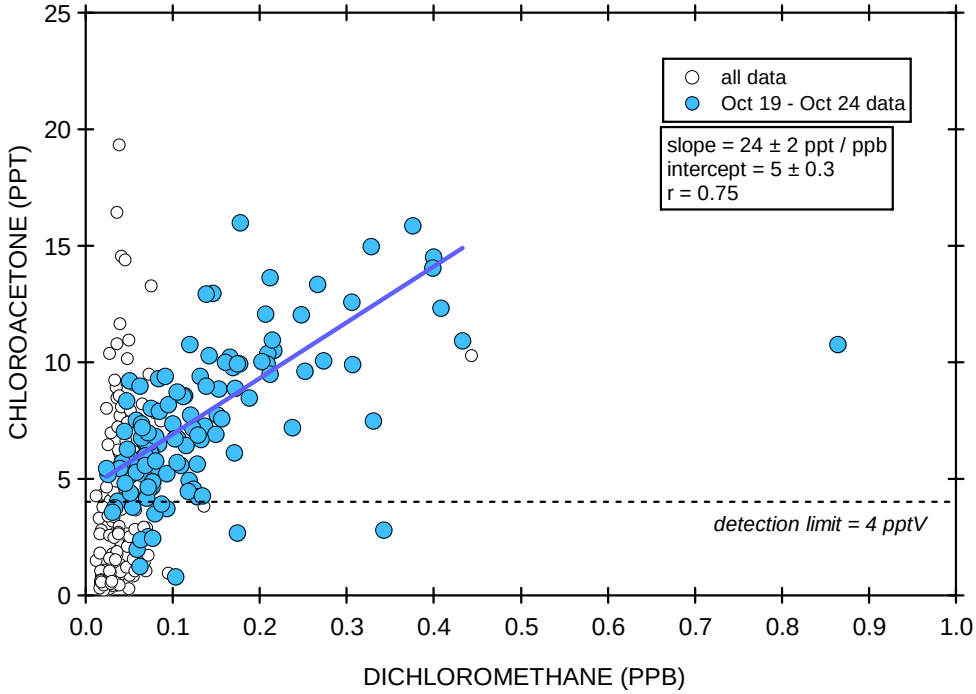

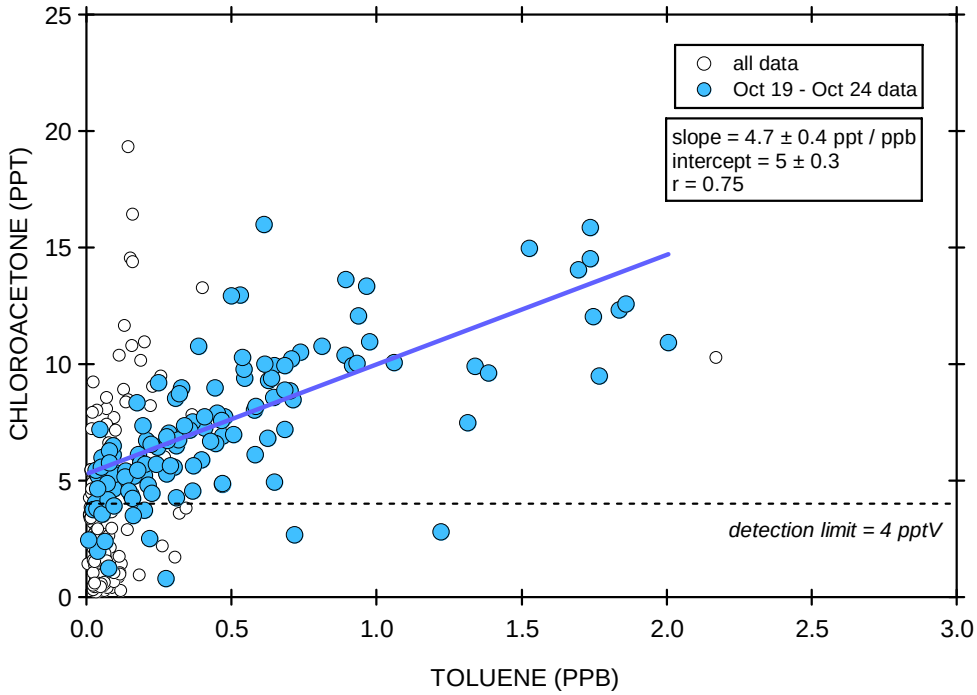

Figure 4.3.11. Zuma Beach data correlations between chloroacetone and a long lived urban air tracer CH_2Cl_2 (upper panel), and a short lived tracer toluene (lower panel). Linear regressions are shown through the LA basin air period from October 19 to October 24 for data above the 4 ppt chloroacetone detection limit.

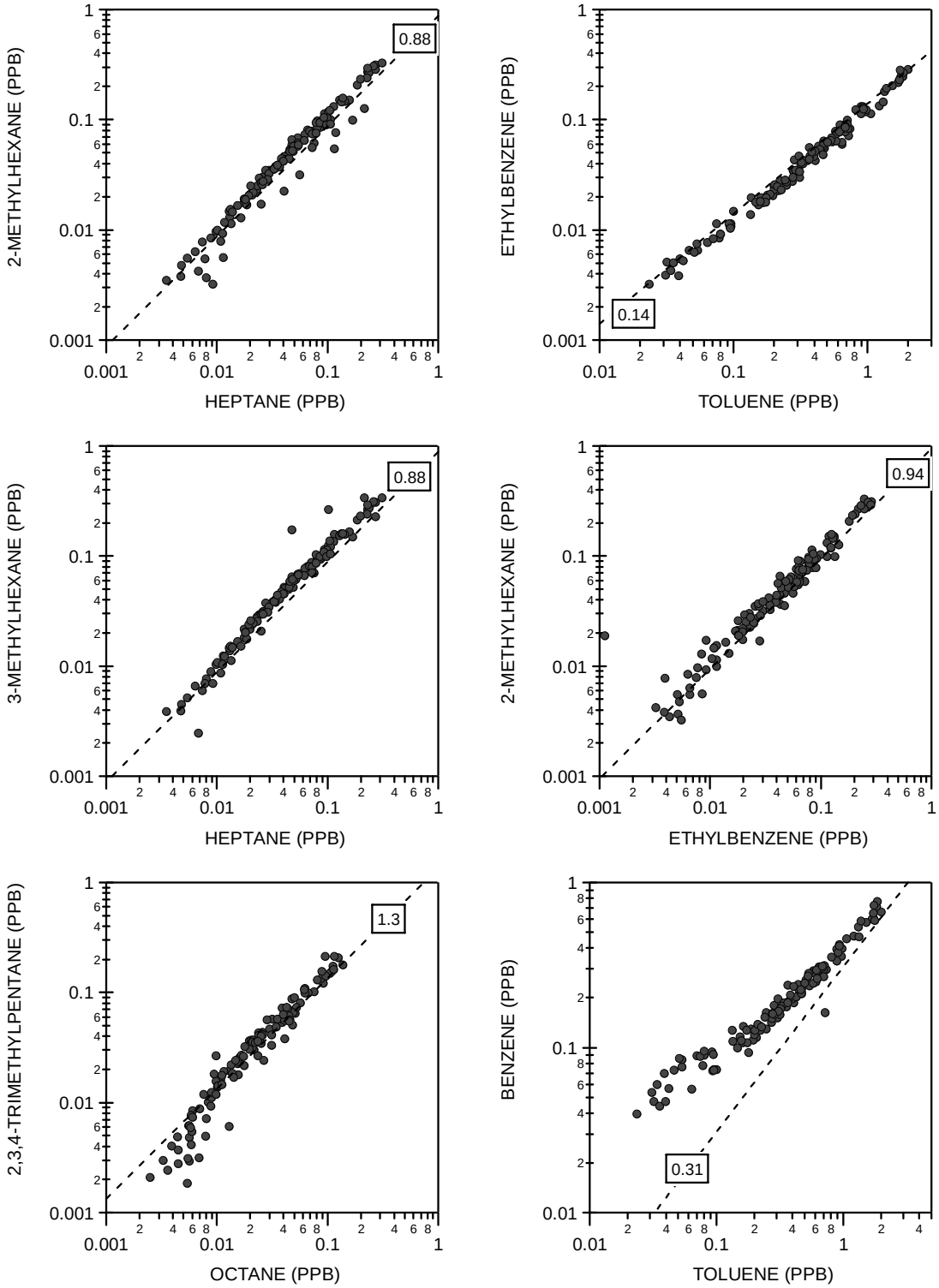

Figure 4.3.12. Correlations between Zuma Beach hydrocarbons with similar OH rate coefficients but significantly different Cl-atom rate coefficients. The data trends are in good agreement with the urban source ratio observed from the CELA canister samples shown as the dashed line.

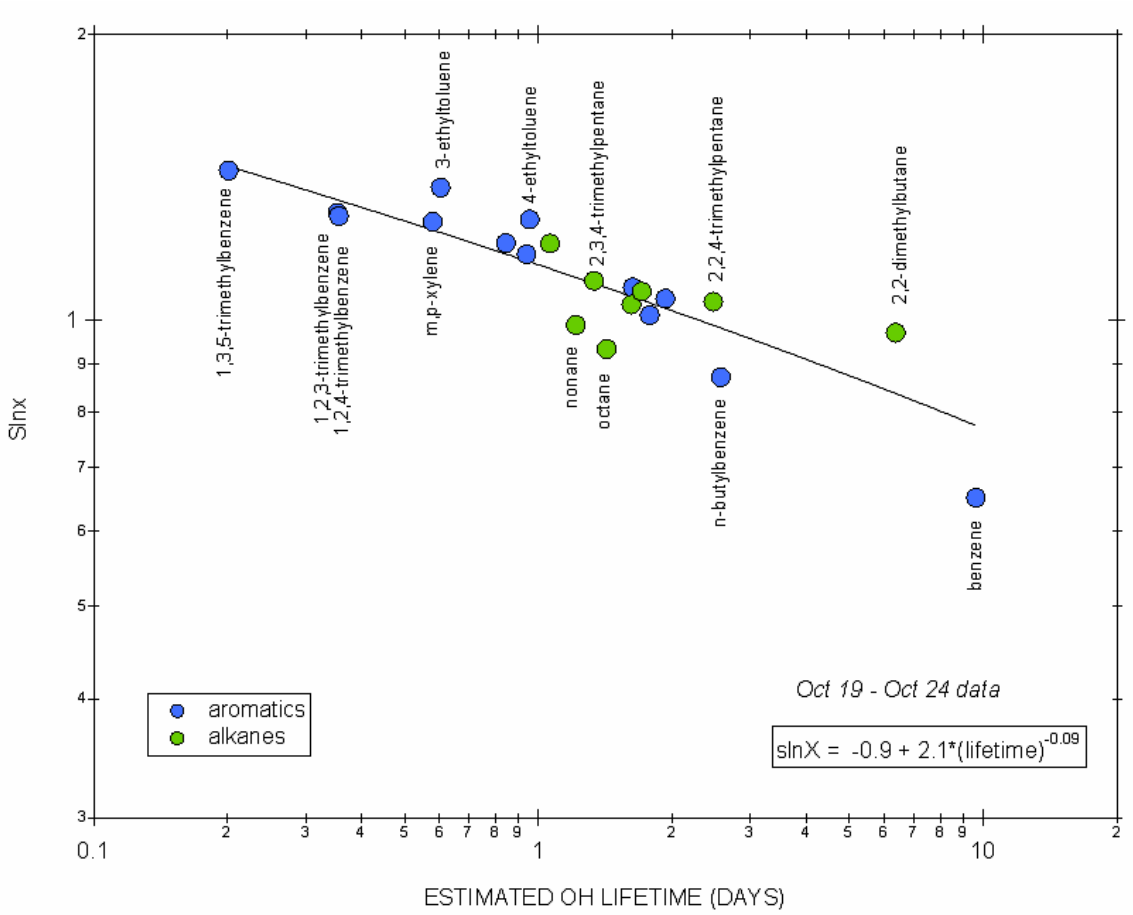

Figure 4.3.13. Measure of variability vs. estimated OH lifetime for hydrocarbons measured by GC-MS at Zuma Beach during the LA basin air outflow period. Plot illustrates only a weak lifetime dependence, indicating that much of the mixing ratio temporal variability was caused by varying degrees of urban plume dilution rather than chemical processing.

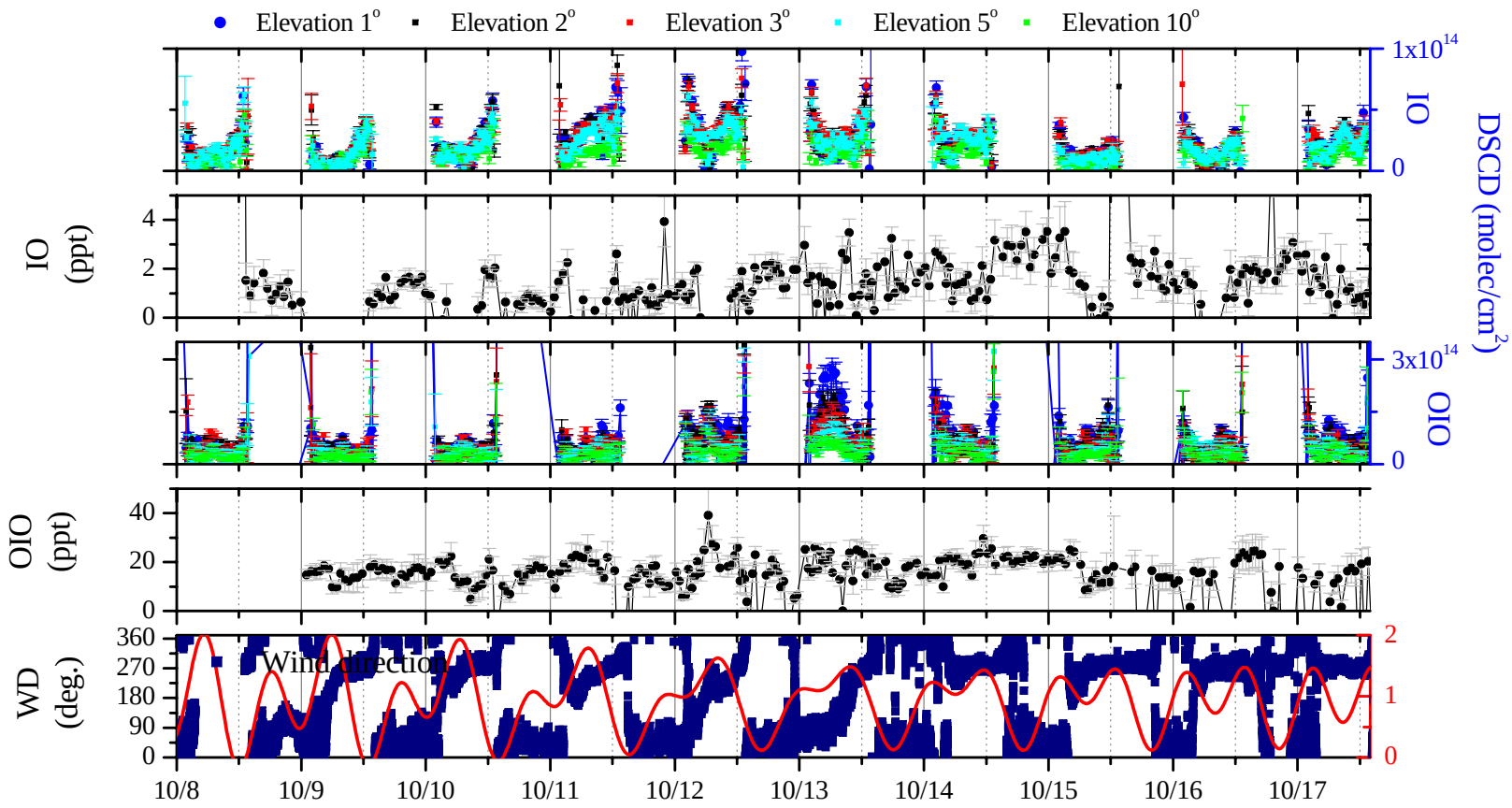

Figure 4.5.1 Overview of observations at Zuma Beach. Top two panels show IO mixing ratios and DSCDs measured by the MAX-DOAS instrument at 1, 2, 3, 5, and 10 degrees elevation viewing angles, and mixing ratios measured by the LP-DOAS respectively. Panels three and four show the same for OIO. Since MAX-DOAS data are only available during the day, it provides orientation for the day and nighttime. The lower panel shows wind direction measured by the UCLA meteorological station at Zuma Beach as well as tidal height.

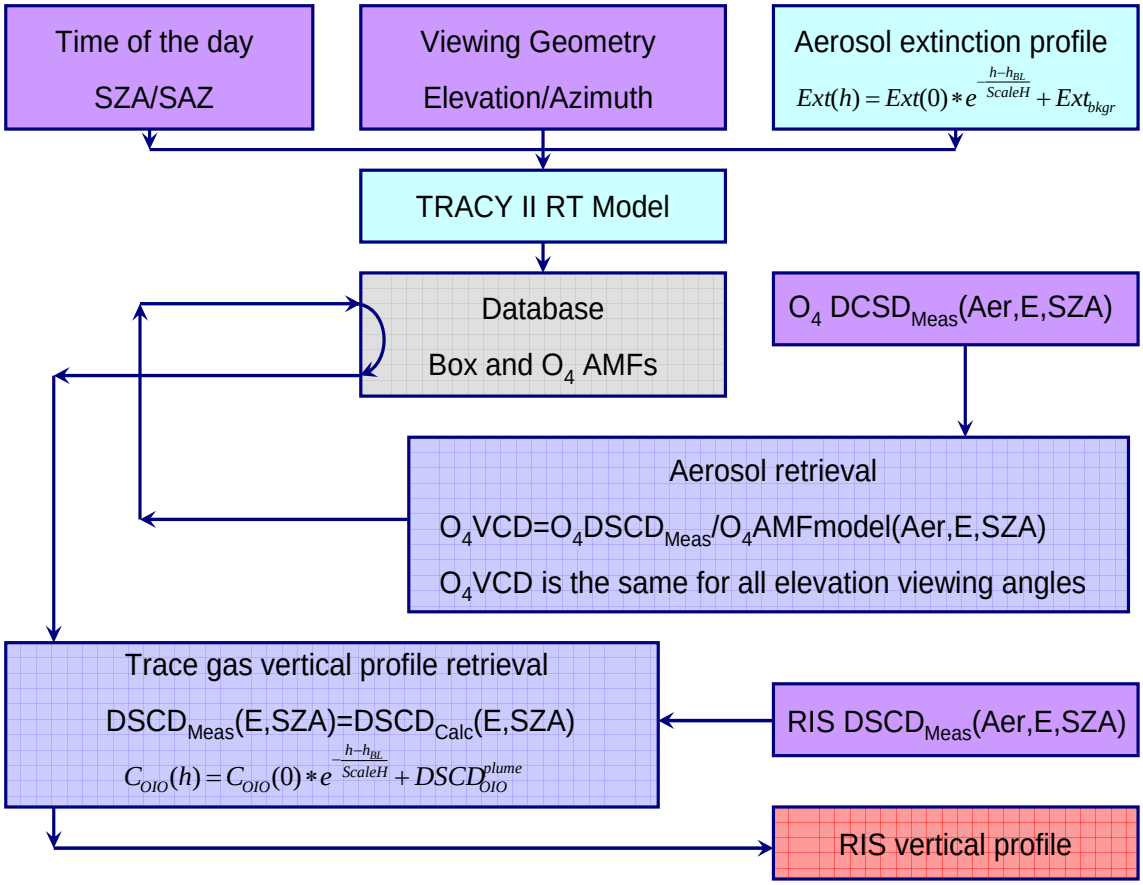

Figure 4.5.2. OIO vertical profile retrieval algorithm.

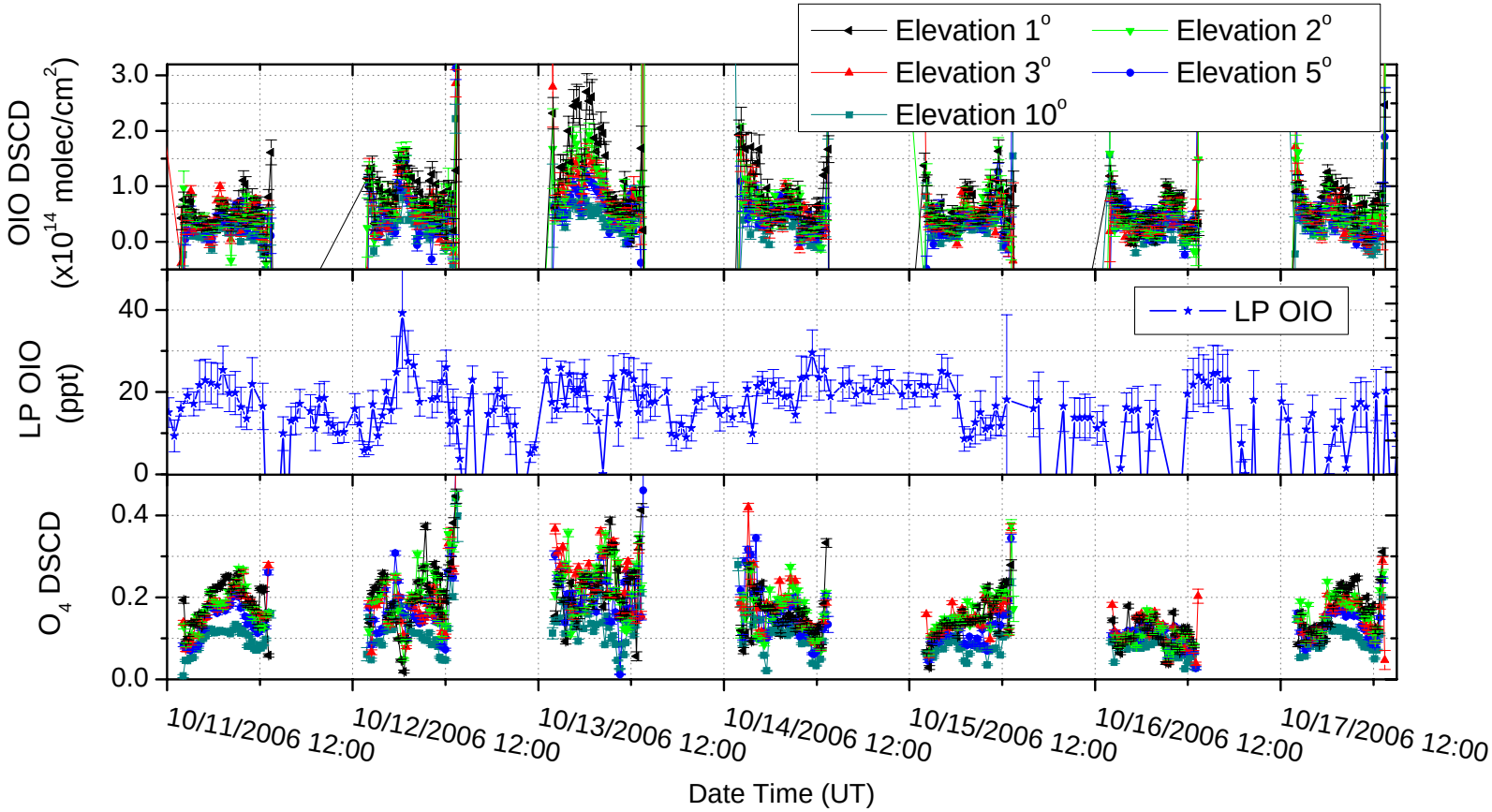

Figure 4.5.3. Zuma OIO DOAS measurement overview. Top panel shows MAX-DOAS OIO DSCDs measured at 1°, 2°, 3°, 5° and 10° elevation viewing angles; middle panel shows LP DOAS OIO mixing ratios; and bottom panel shows MAX-DOAS O_4 DSCDs from the 530 nm center wavelength spectra for all five elevation viewing angles.

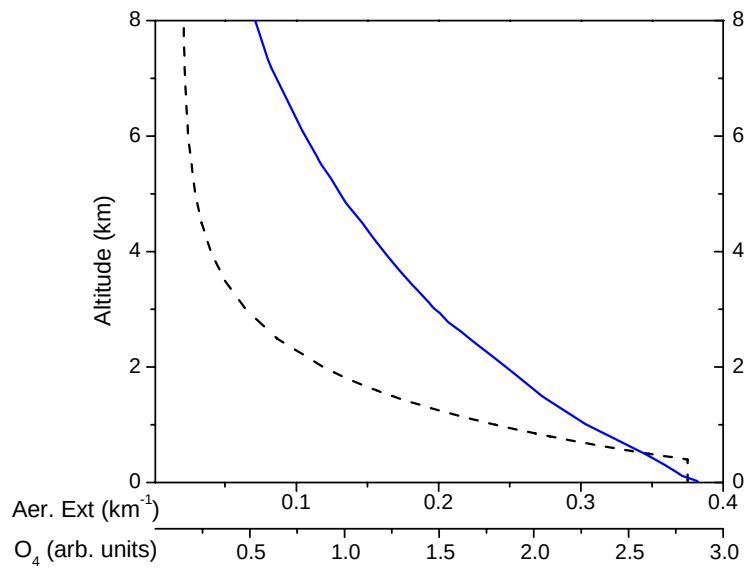

Figure 4.5.4. Example of an aerosol profile (dashed black line) generated during the aerosol retrieval process and the O_4 vertical profile (solid blue line) used for RT calculations. Parameters for this aerosol profile are H_{BL}= 400 m; Ext_{BL} = 0.355 km^{-1}; *ScaleH* = 1; Ext_{Bckgr} = 0.02 km^{-1}. O_4 profile was constructed using atmospheric T and P vertical profiles. For Zuma Beach, profiles collected by airplanes on approach to LAX were used [provided by ACARS database http://www.acarsd.org/].

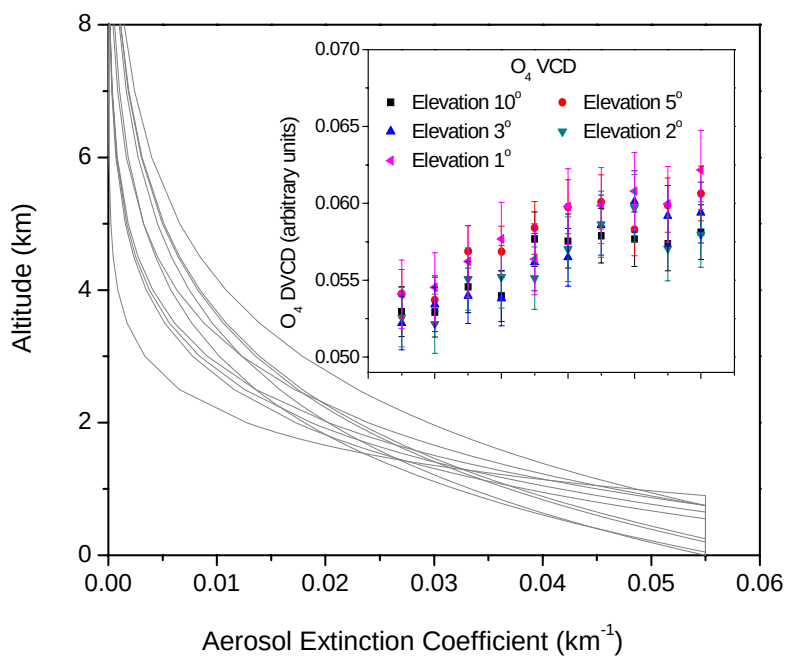

Figure 4.5.5. Example of the aerosol profile retrieval. Gray lines show aerosol profiles that satisfy requirement for O_4 VCDs for all elevations to be equal within errors. This is illustrated in the inset figure that shows O_4 VCDs for all presented aerosol profiles. For each of the profile, VCDs at all elevation viewing angles agree within the error bars.

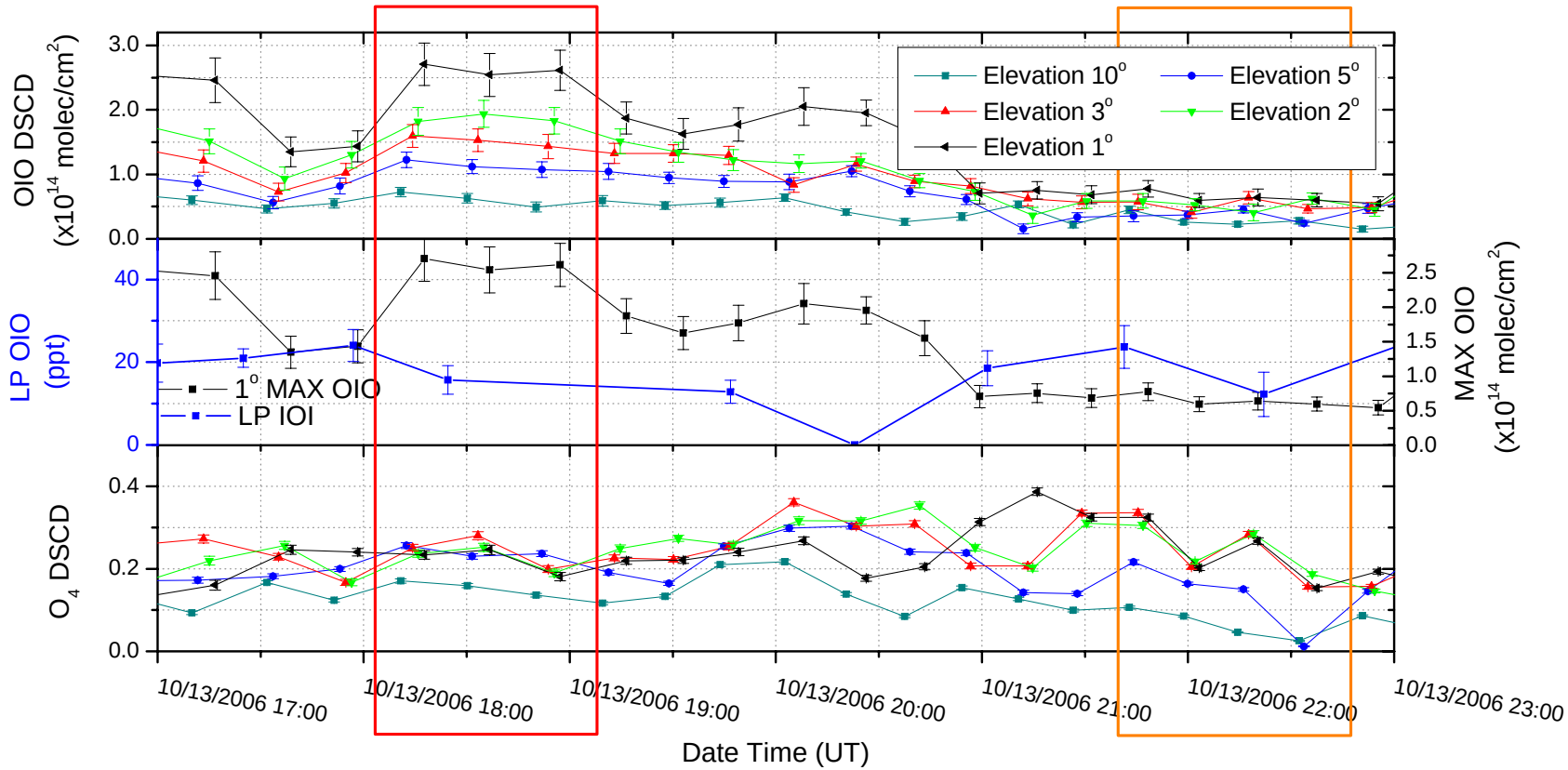

Figure 4.5.6. Overview of OIO MAX- and LP DOAS measurements on October 13, 2006. See text for description of outline boxes.

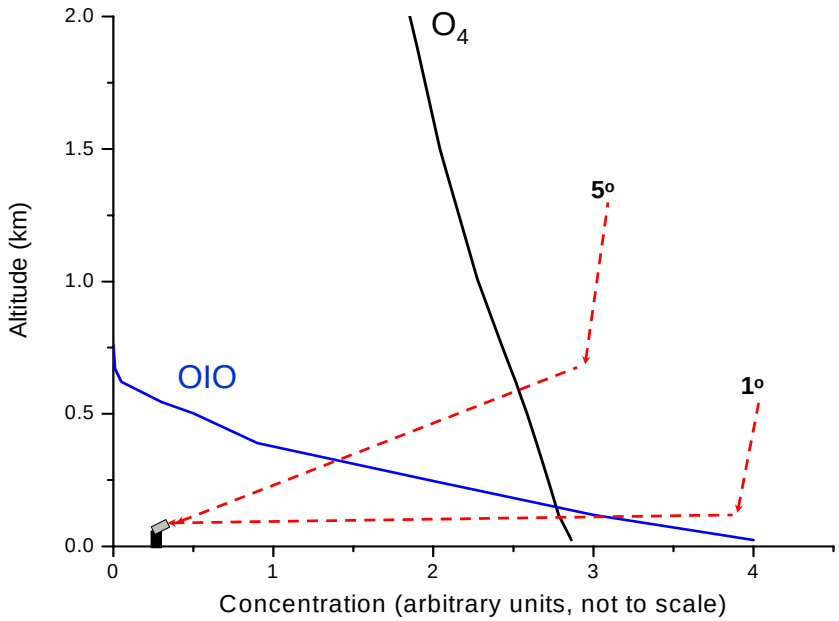

Figure 4.5.7. Schematic representation of MAX-DOAS light paths for 1° and 5° elevation viewing angles (dashed lines). The O_4 atmospheric profile (black line) slowly changes with altitude and the hypothetical OIO profile (blue line) is very close to the surface.

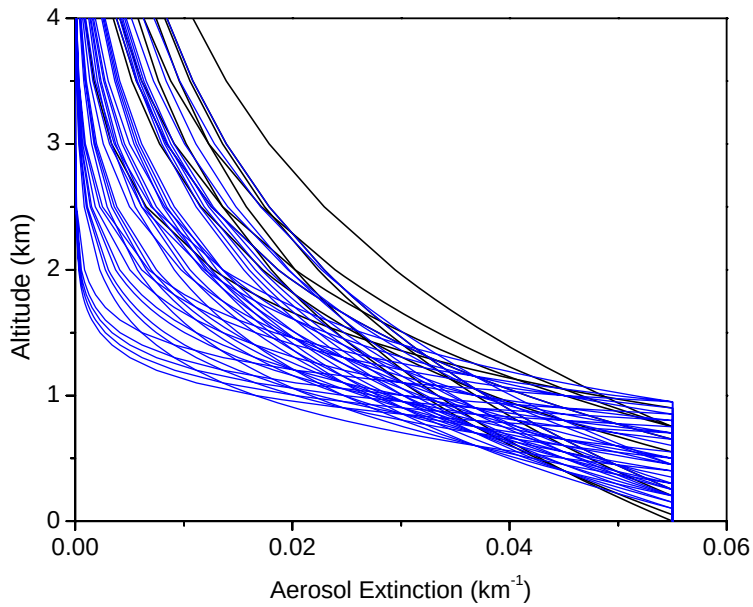

Figure 4.5.8. Aerosol retrievals for October 13, 2006 between 18:10 and 18:30 UT in Malibu, CA.

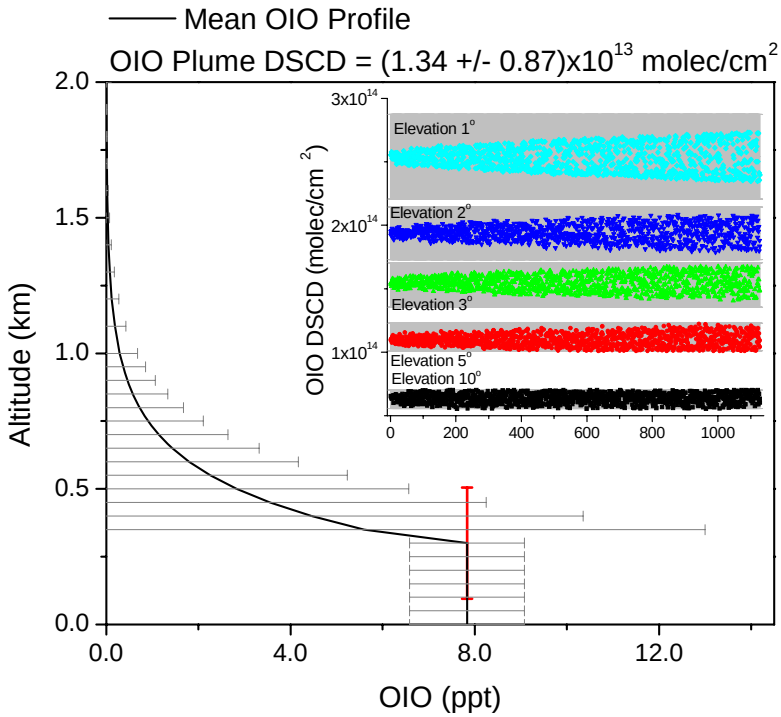

Figure 4.5.9. OIO vertical profile retrieved for October 13, 2006 at 18:30 UT. In addition to the homogeneous profile showed here, there is also 1.34 (± 0.87) × 10^{13} molec/cm^2 OIO present in the marine boundary layer in the inhomogeneous plumes.

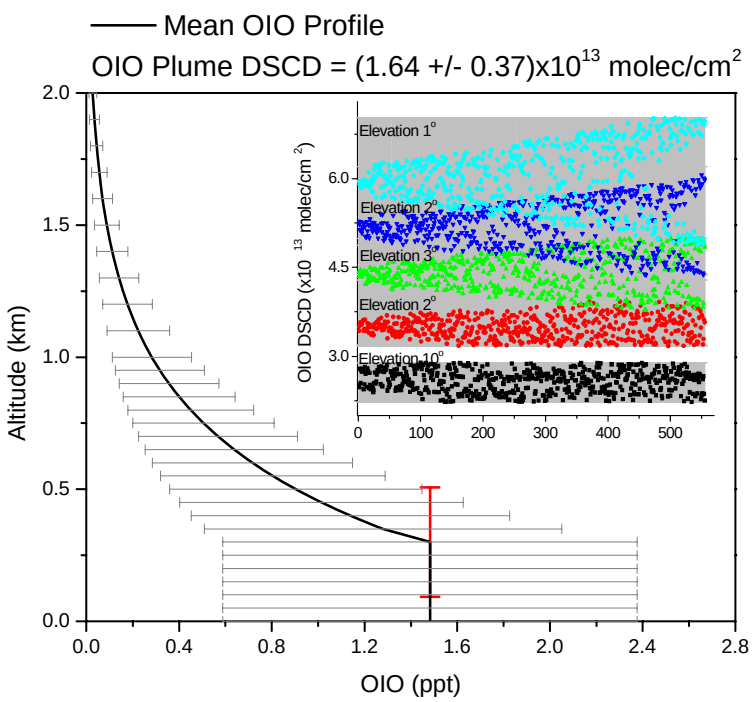

Figure 4.5.10. OIO vertical profile retrieval for October 13, 2006 at 22:03 UT. In addition to the homogeneous profile showed here, there is also 1.64 (± 0.37) × 10^{13} molec/cm^2 OIO present in the marine boundary layer in the inhomogeneous plumes.

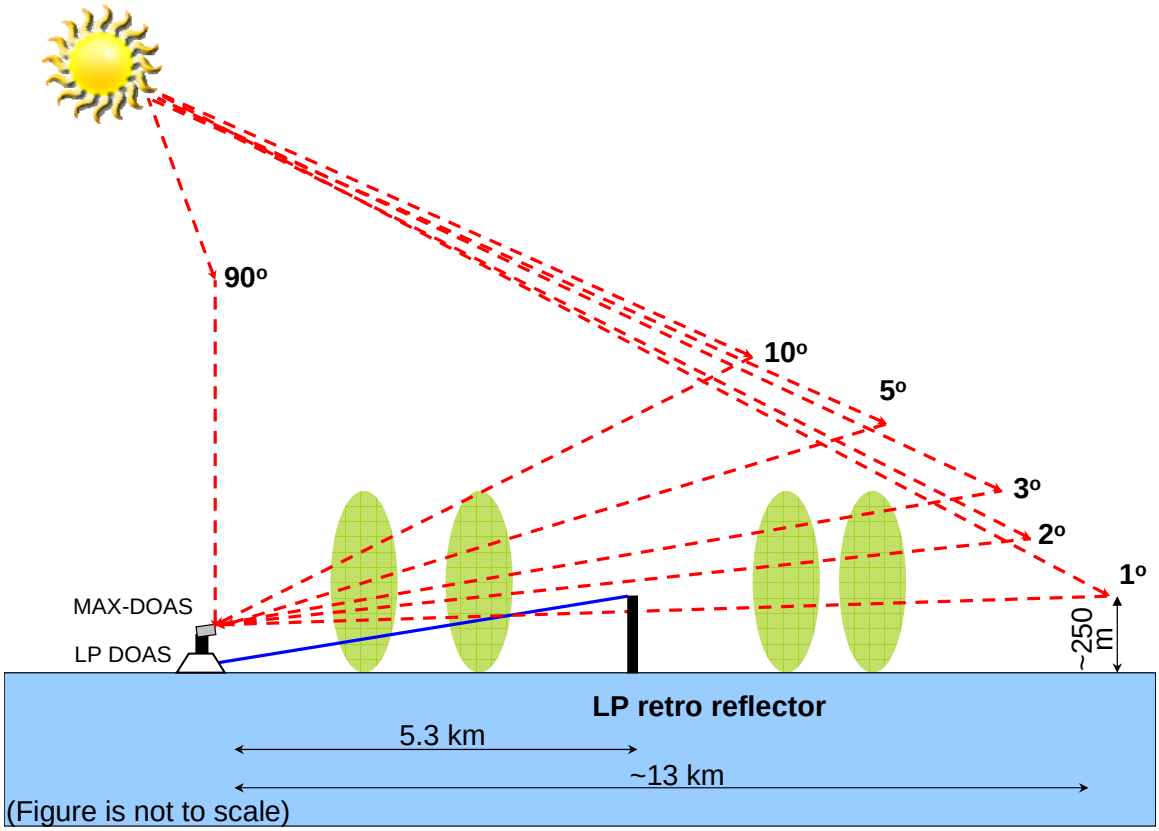

Figure 4.5.11. Schematics of the OIO spatial distribution model. Blue line represents LP DOAS light path between the Zuma and El Matador Beach, red dashed lines represent MAX-DOAS lines of sight at different elevation viewing angles. Green ovals represent inhomogeneous IO plumes.

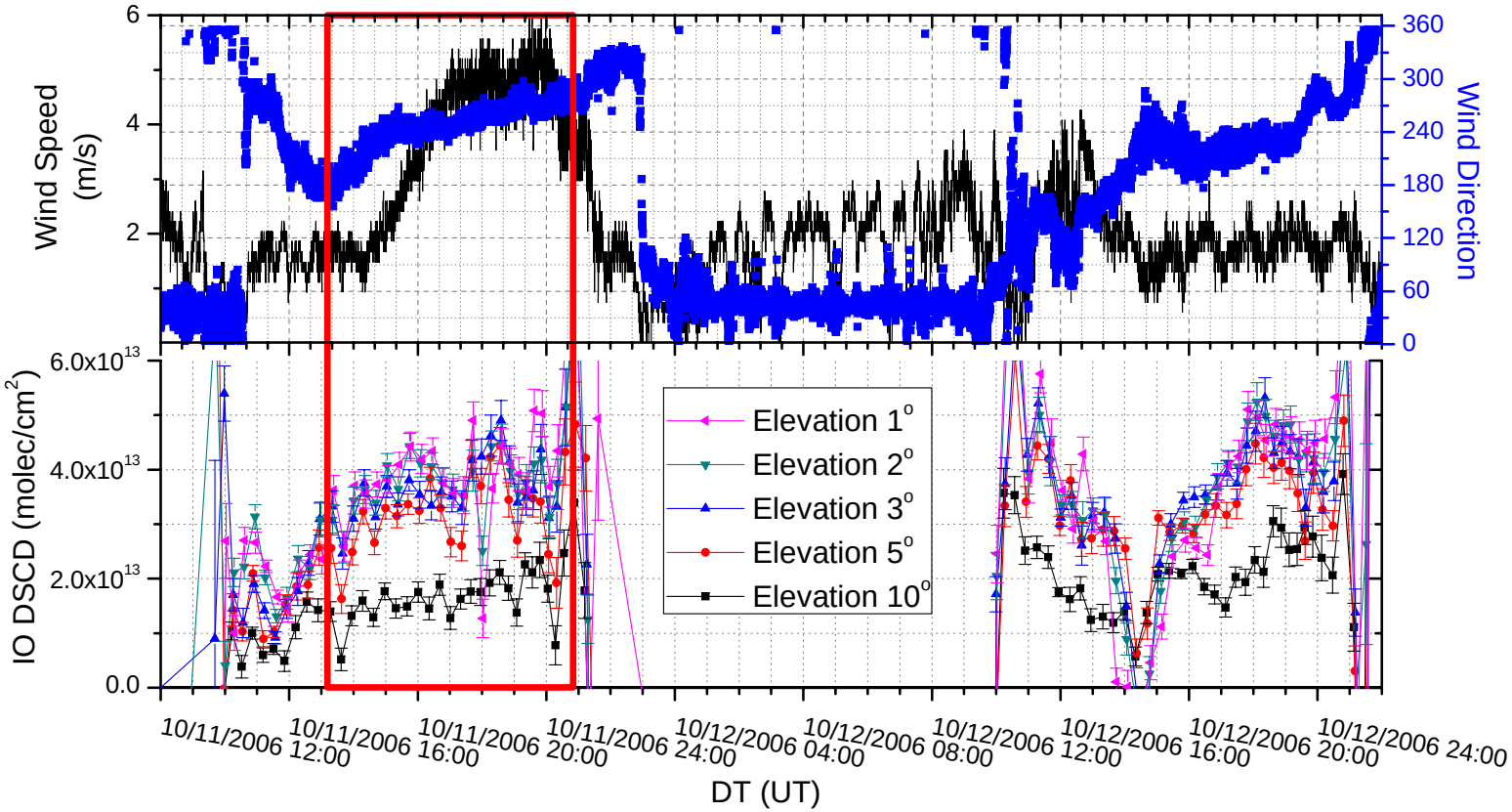

Figure 4.5.12. MAX-DOAS IO DSCDs and wind speed and direction at Zuma Beach on October 11 and 12, 2006. See text for description of outline box.

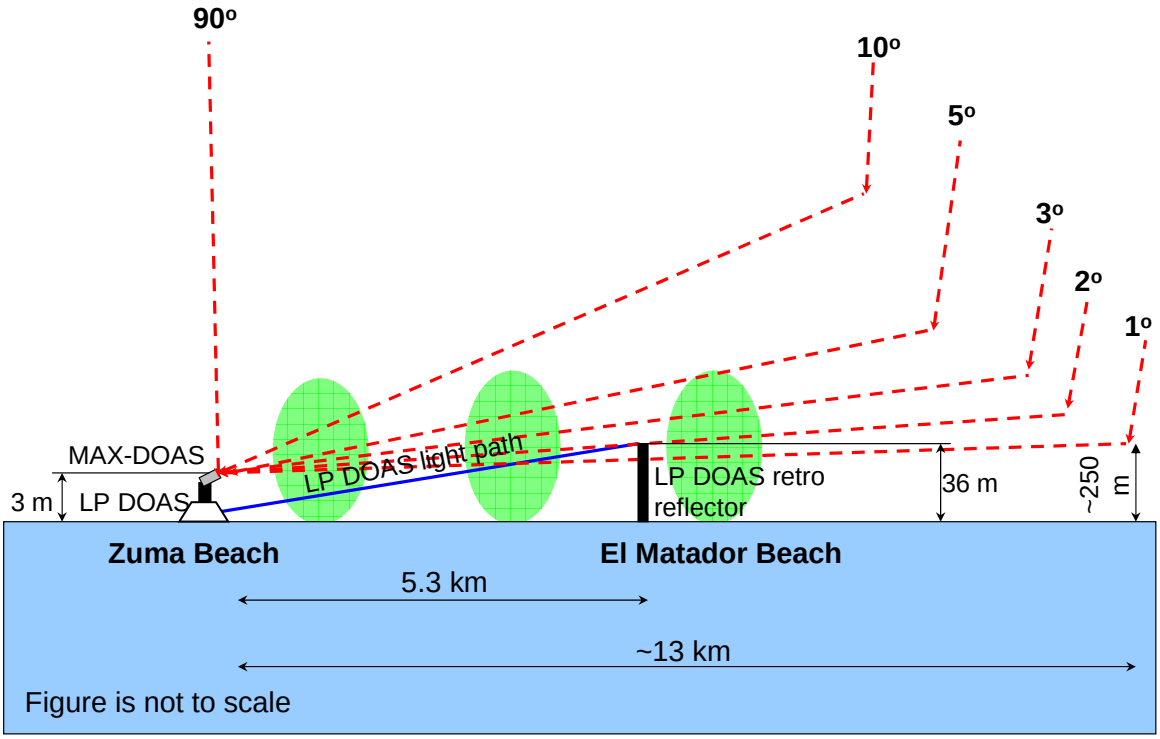

Figure 4.5.13. Schematics of IO spatial distribution at Zuma Beach. Blue line represents LP DOAS light path between the Zuma and El Matador Beach, red dashed lines represent MAX-DOAS lines of sight at different elevation viewing angles. Green ovals represent inhomogeneous IO plumes.

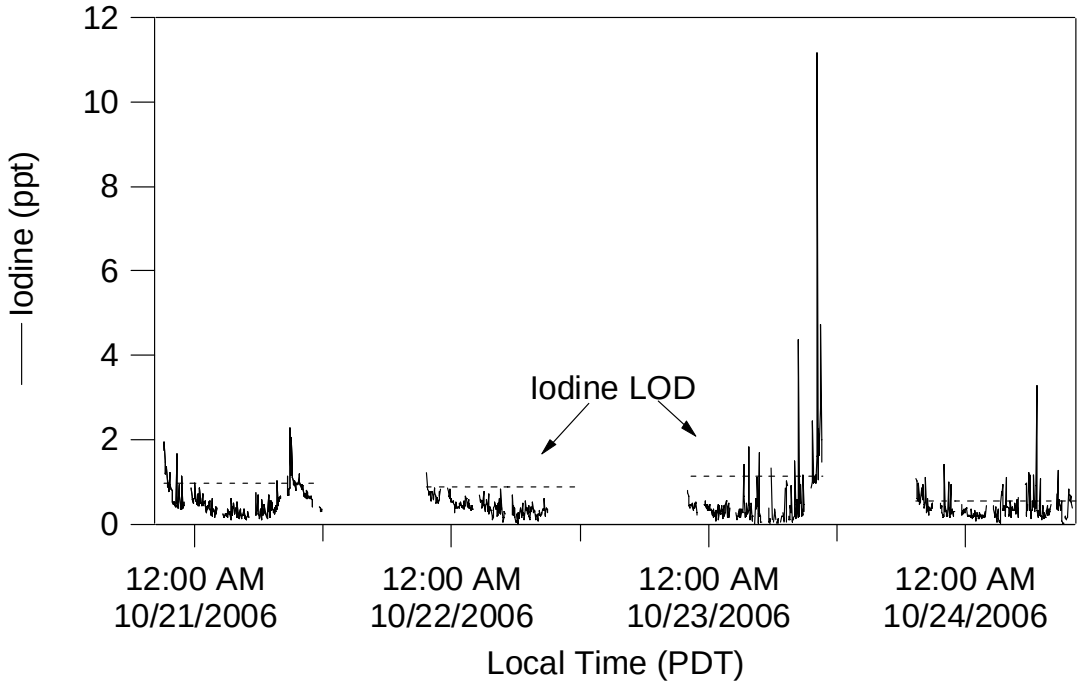

Figure 4.6.1. Battelle ambient I_2 dataset. The solid trace shows the I_2 measurements and the dashed line shows the LOD for each day

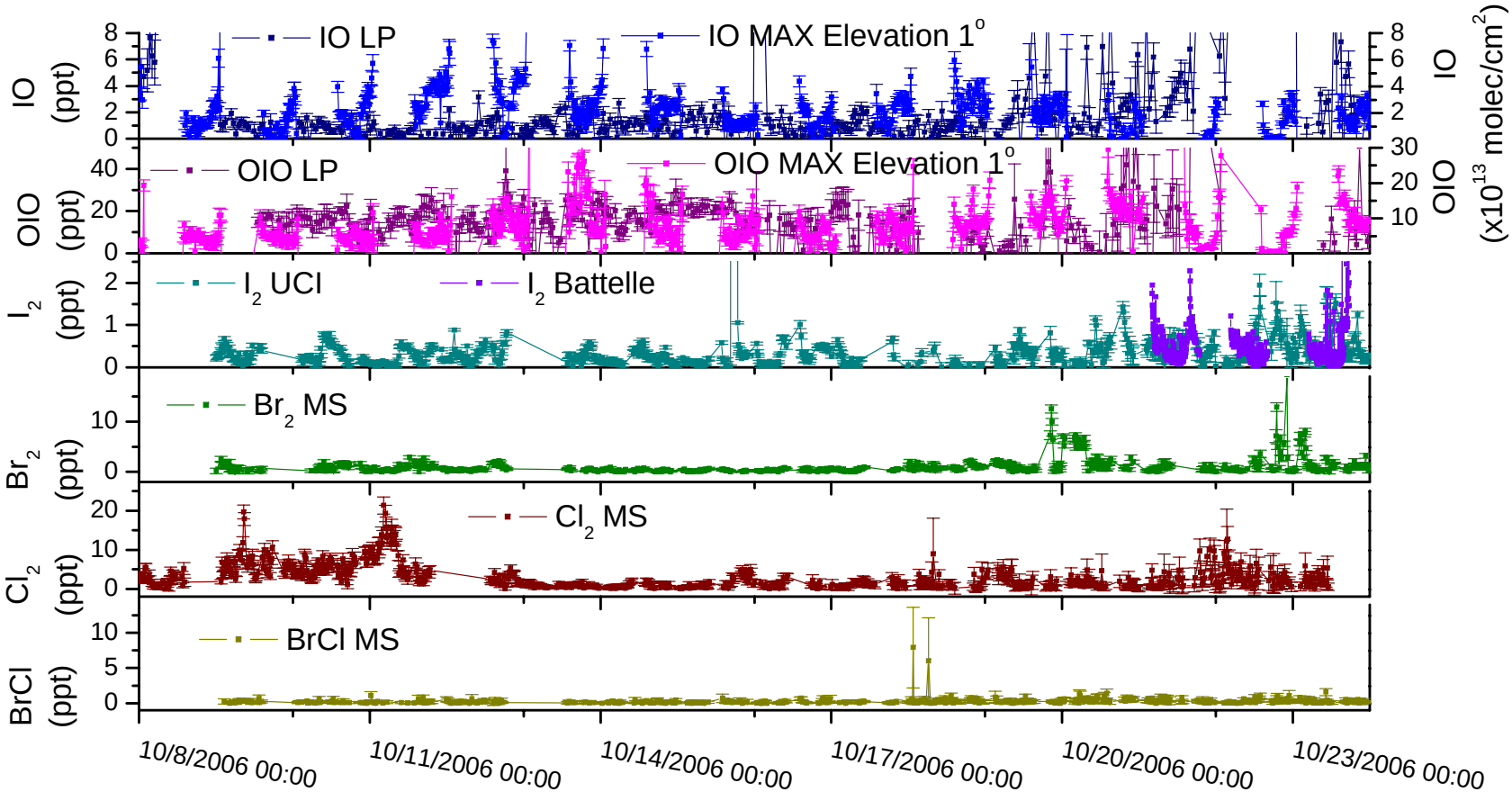

Figure 4.6.2 Overview over all halogen species detected at Zuma Beach. The plot contains the observations from UCLA's DOAS instruments, Battelle's API-MS/MS, and UCI's MS.

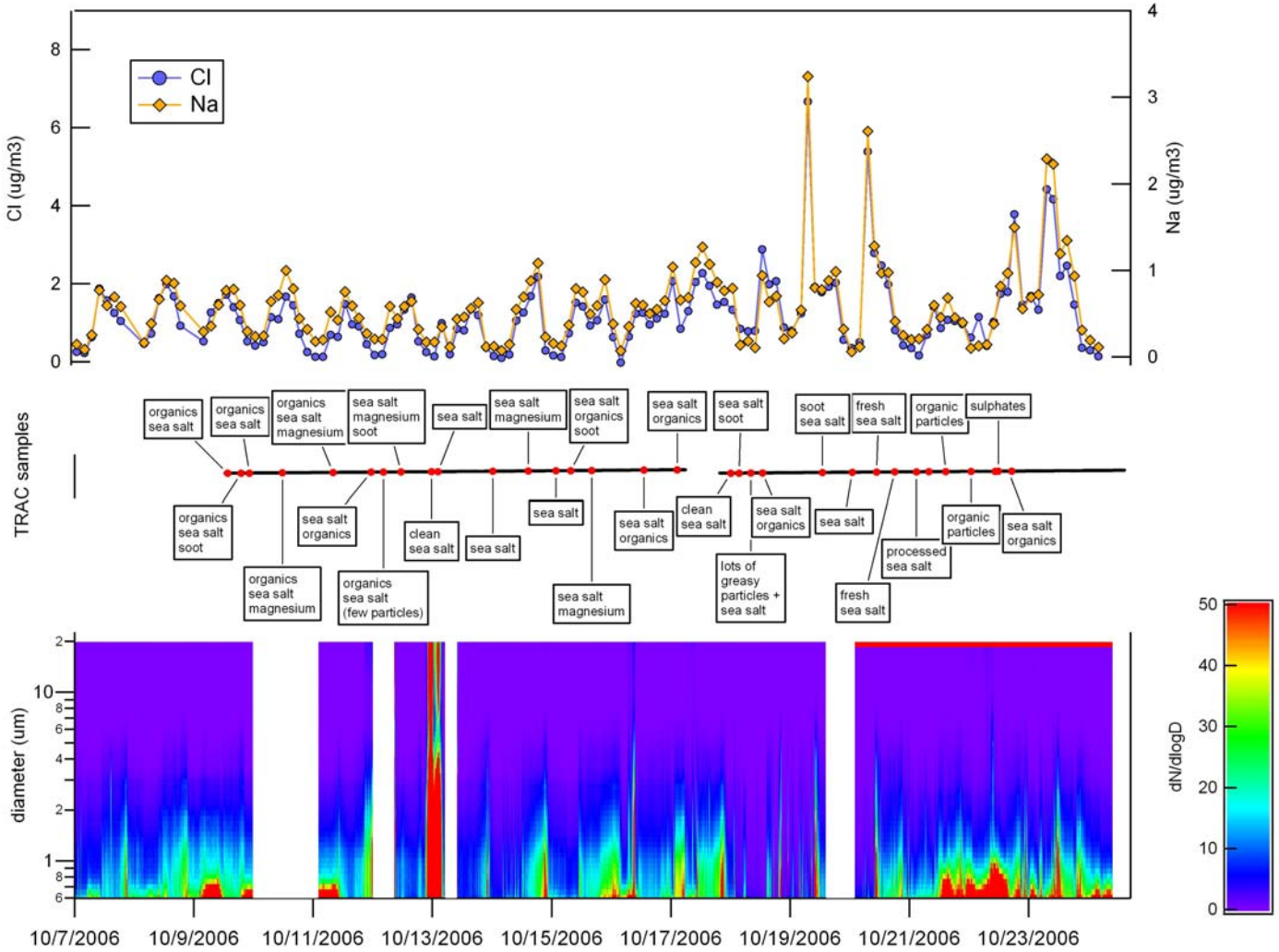

Figure 4.7.1 Aerosol size distribution, TRAC sample particle morphology observations, and Na and Cl aerosol concentrations.

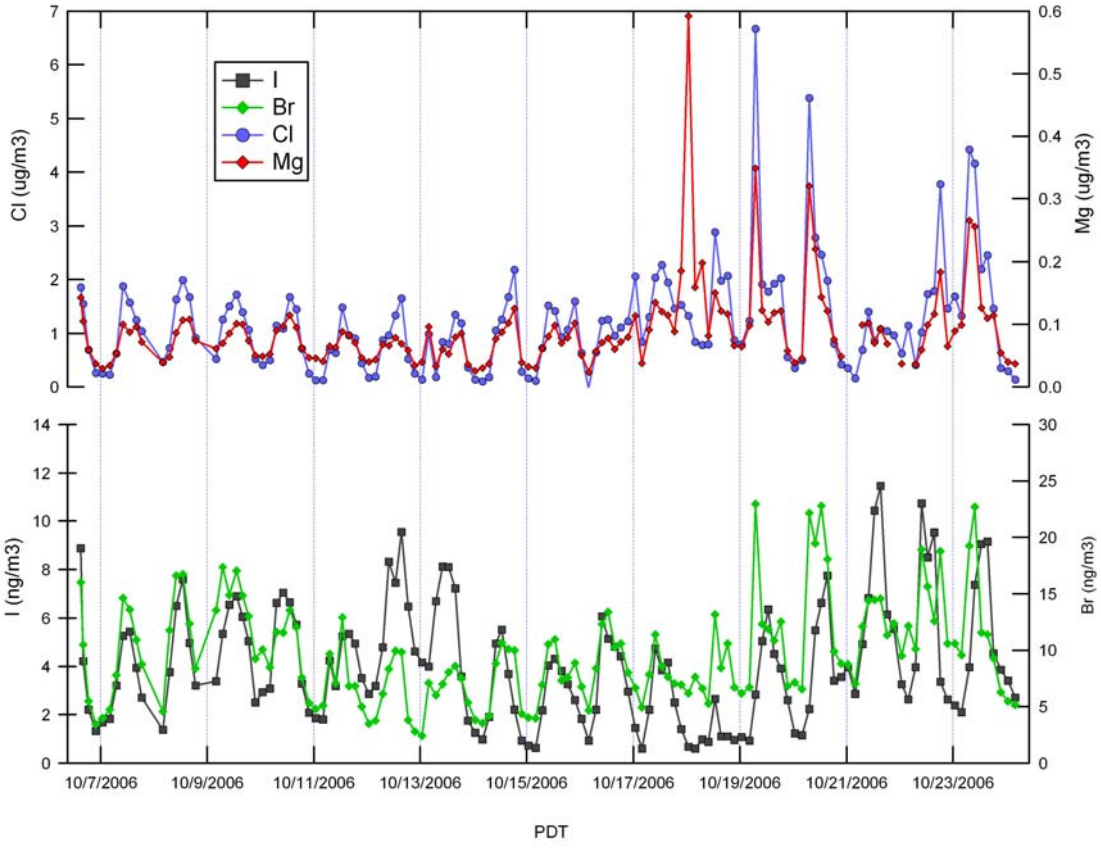

Figure 4.7.2 Particulate composition of major and minor elements associated with sea-salt particles (A. Pszenny, UNH)

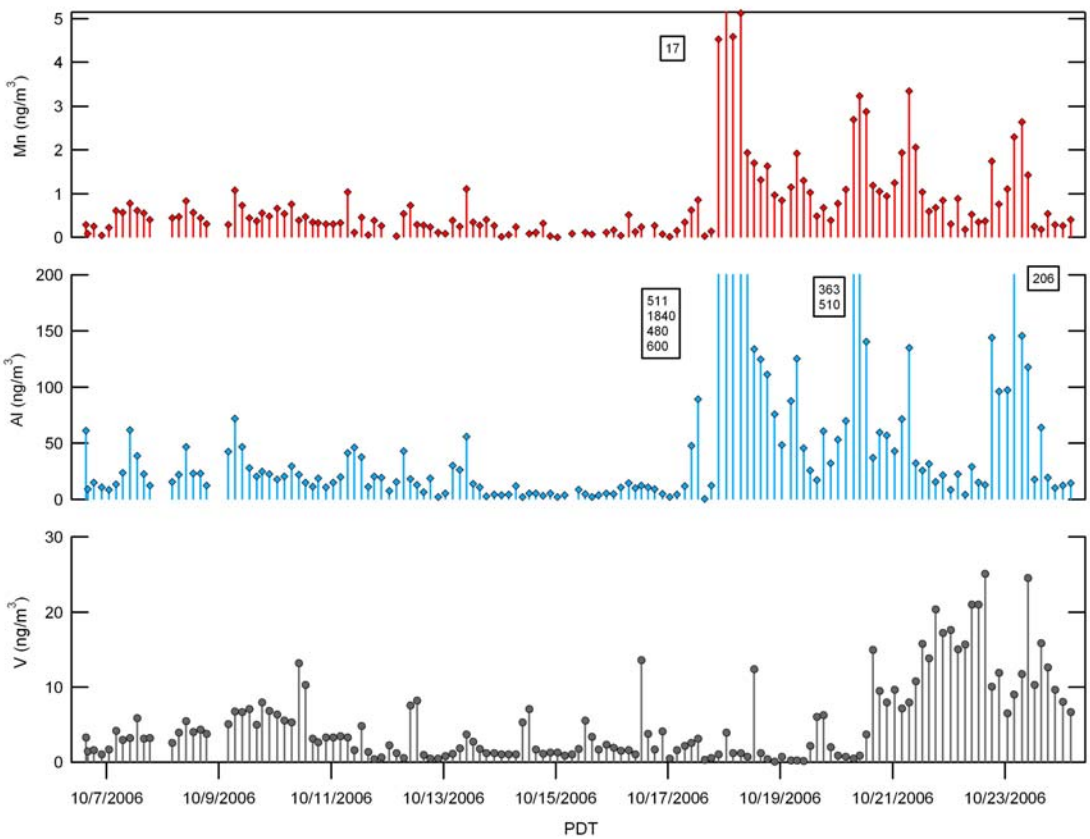

Figure 4.7.3 Particulate trace metal concentrations. Values of offscale data are listed as boxed values (A. Pszenny, UNH)

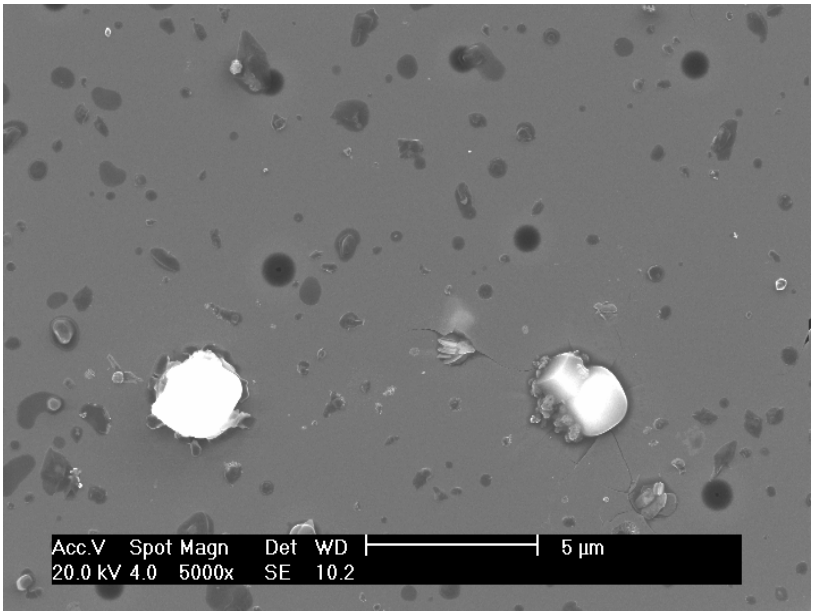

Figure 4.7.4 SEM image of particles collected by TRAC from October 9 22:21 (Disk 1, hole 33) showing fresh sea-salt particles (large white objects) and organic particles (darker objects).

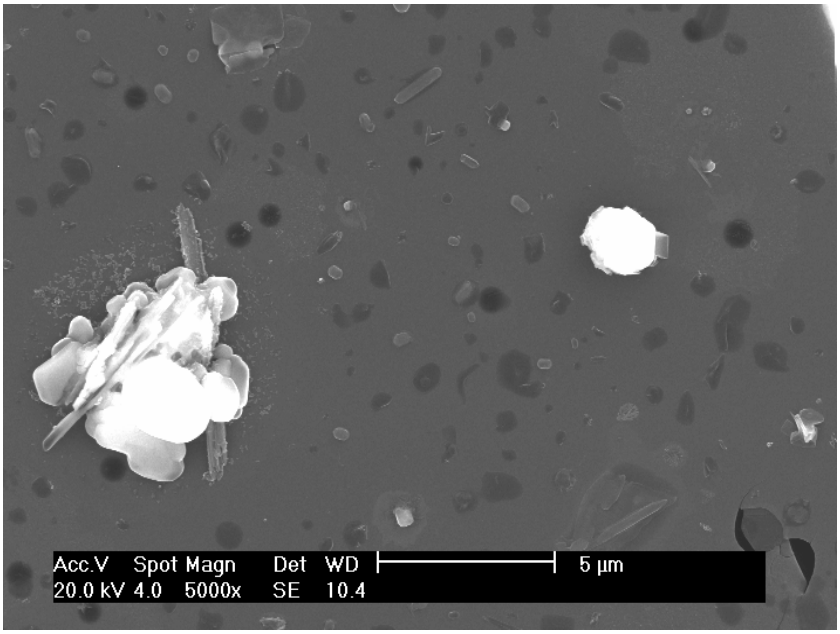

Figure 4.7.5 SEM image of particles collected by TRAC from October 10 11:42 (Disk 1, hole 72) showing chemically processed sea-salt particles (sodium sulfate).

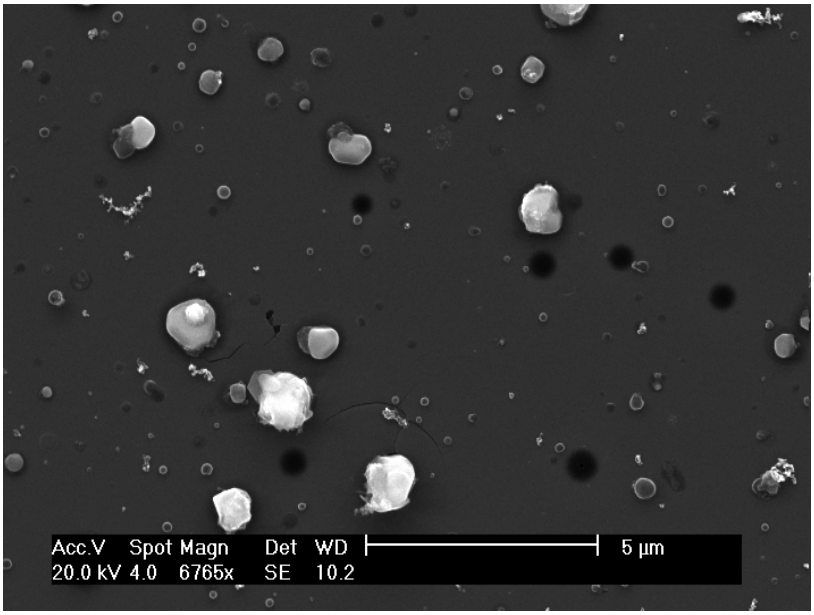

Figure 4.7.6 SEM image of particles collected by TRAC from October 19 13:03 (Disk 2, hole 131) showing fresh and chemically processed sea-salt particles and soot particles.

Chapter 5

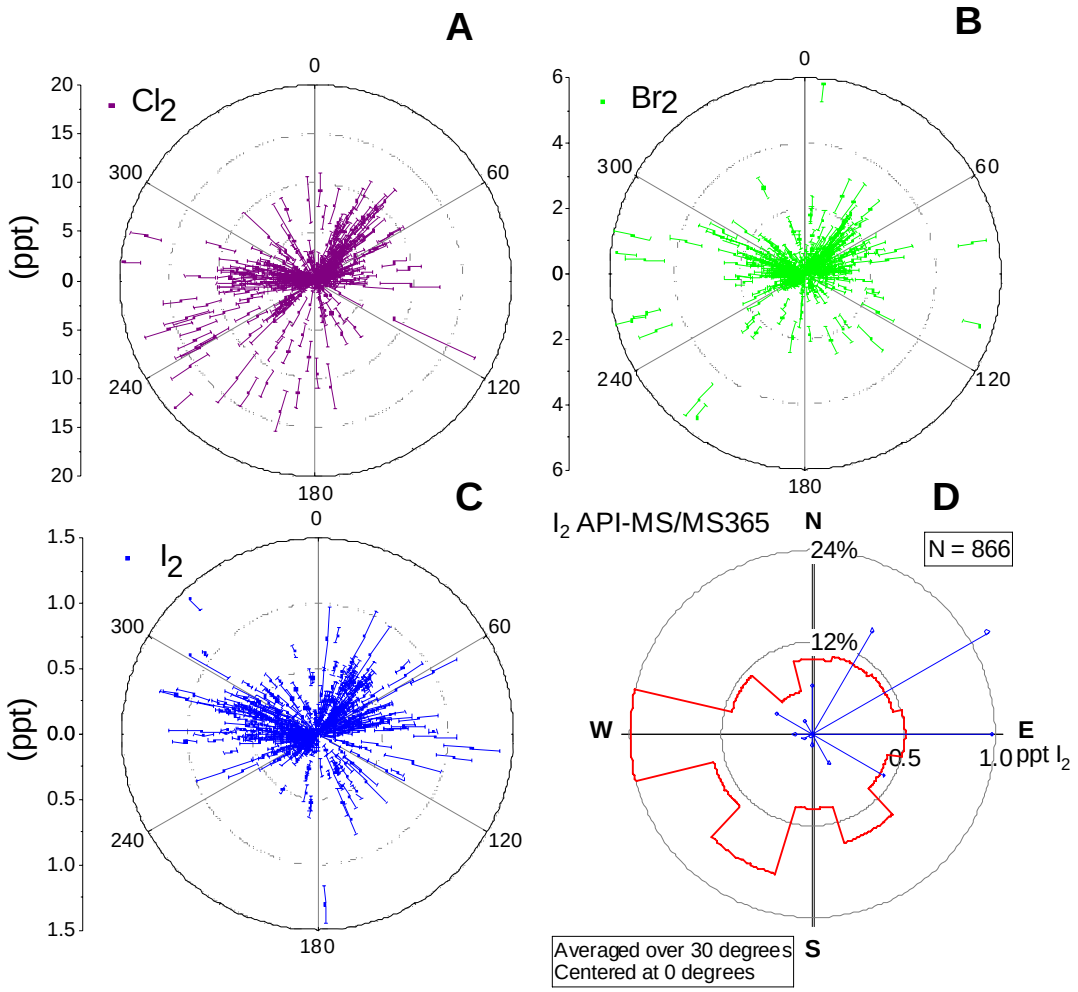

Figure 5.1.1 Dependence of molecular halogens (Cl_2, Br_2, and I_2), as measured by the UCI MS instrument, on wind direction (A-C). Panel D shows a wind rose plot of ambient I_2 measured by the API-MS/MS, where the I_2 mixing ratios (red trace) were averaged over 30 degree wind direction bins and plotted as a function of wind direction on a polar axis. The blue lines represent the frequency of observations in each wind direction bin by percent.

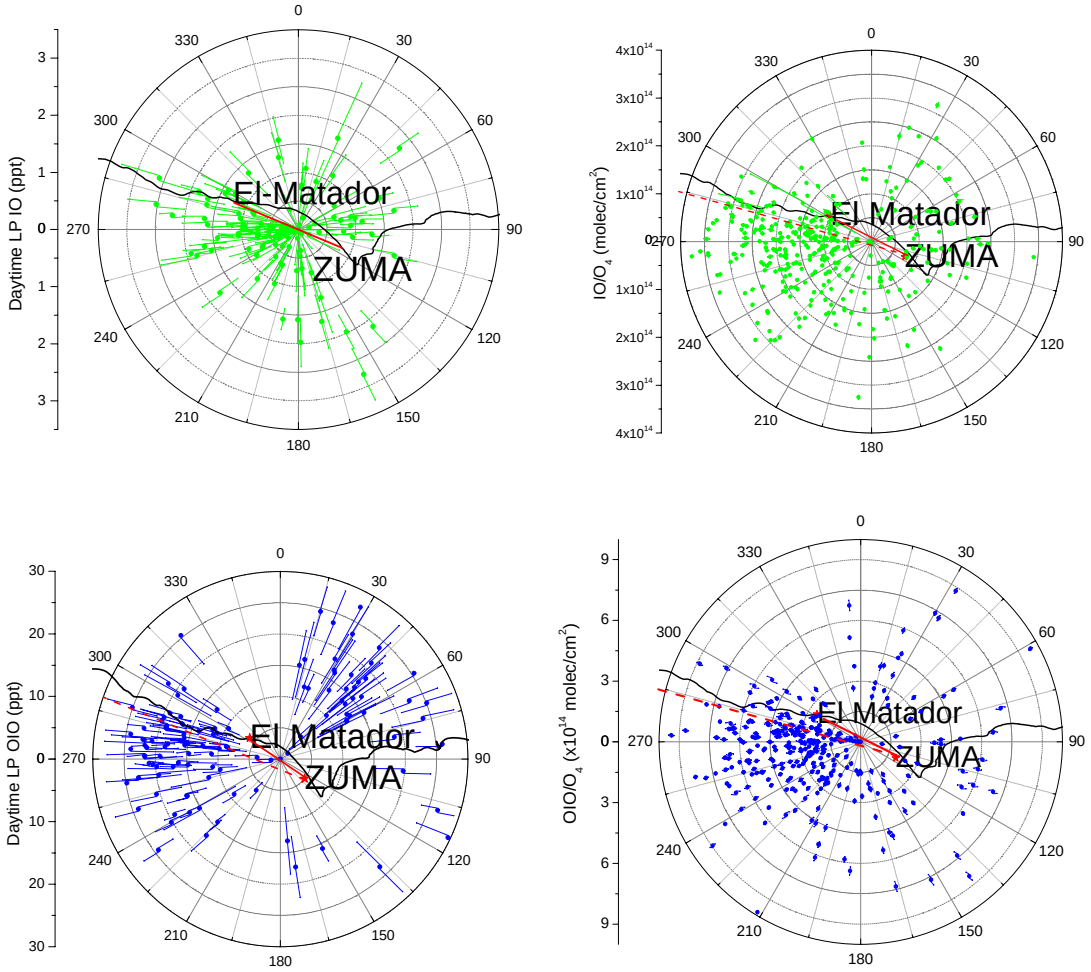

Figure 5.1.2. Daytime IO and OIO mixing ratios (ppt) (left panels) and IO/O_4 and OIO/O_4 ratios (right panels) as a function of wind direction in Malibu.

Figure 5.1.3. Map of the Southern California coastline and neighboring islands. Zuma Beach measurements location is marked by the yellow star. Directly west of Zuma Beach are Channel Islands, and Santa Catalina Island is to the south-east. Distance to both islands from Zuma Beach is approximately 65 kilometers (40 miles).

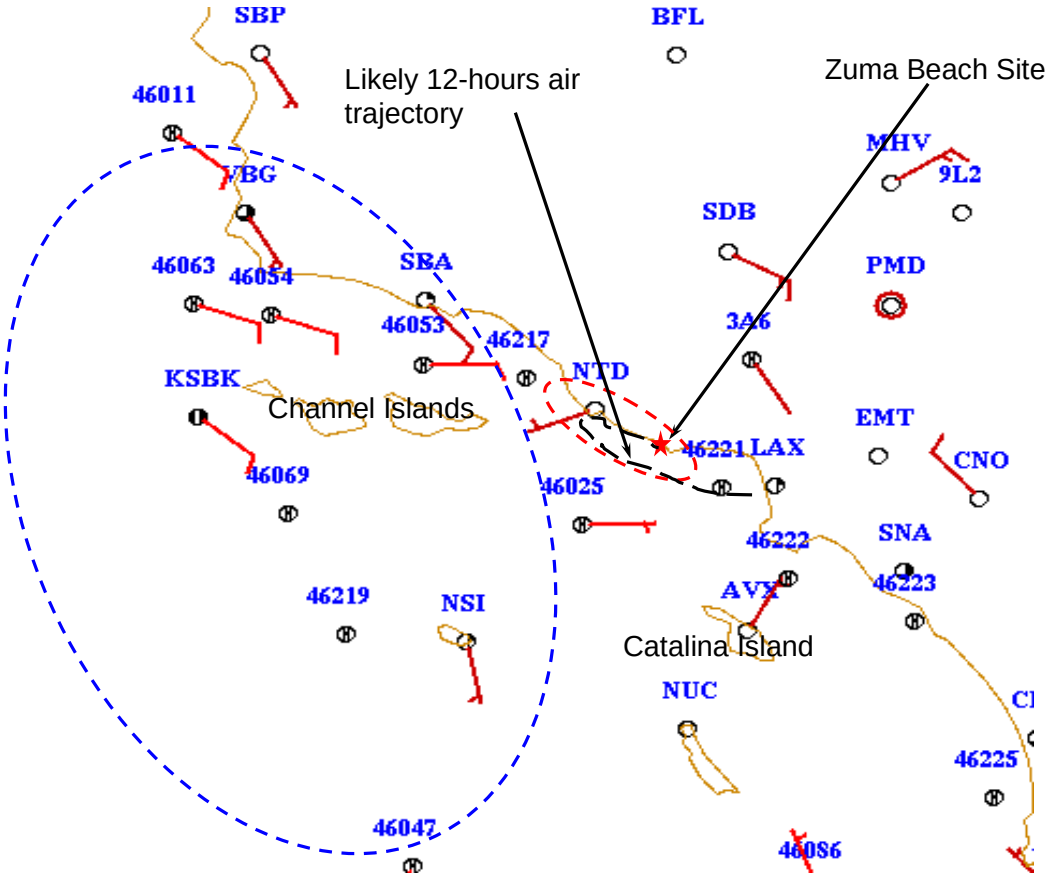

Figure 5.1.4. Wind data reported by weather stations around Southern California coast at 18:00 UT on October 11, 2006. Zuma Beach measurement site is marked by the red star. Blue dashed line represents off-coast cyclonic system that led to the easterly winds observed for the south-east part of LA Basin, off-shore islands and Santa Barbara County. Red dashed line represents areas unaffected by the off-shore cyclone.

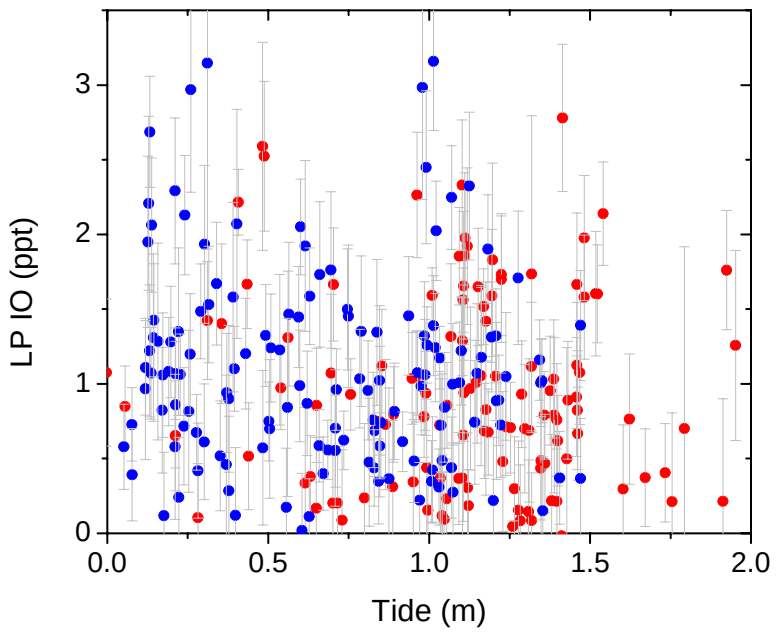

Figure 5.1.5. Observed relationship between the IO measured by the LP DOAS and tidal height in Malibu. Red points represent daytime and blue points nighttime IO measurements.

Figure 5.2.1. Photograph of macroalgae *Macrocystis pyrifera*, Coralline, and Surf grass found on the Zuma Beach in October of 2006.

Figure 5.2.2. Photograph of the kelp emission experiment. As shown, the Teflon bag was being inflated with zero air (*i.e.*, the vent tube was capped).

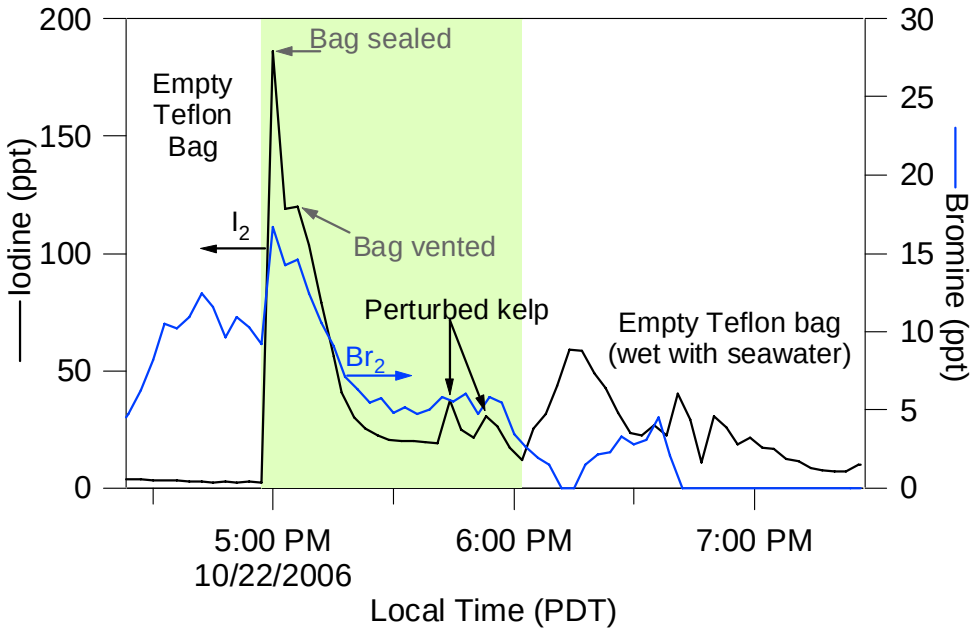

Figure 5.2.3. I_2 emission from kelp while enclosed in a Teflon bag. Also shown are Br_2 measurements during the experiment.

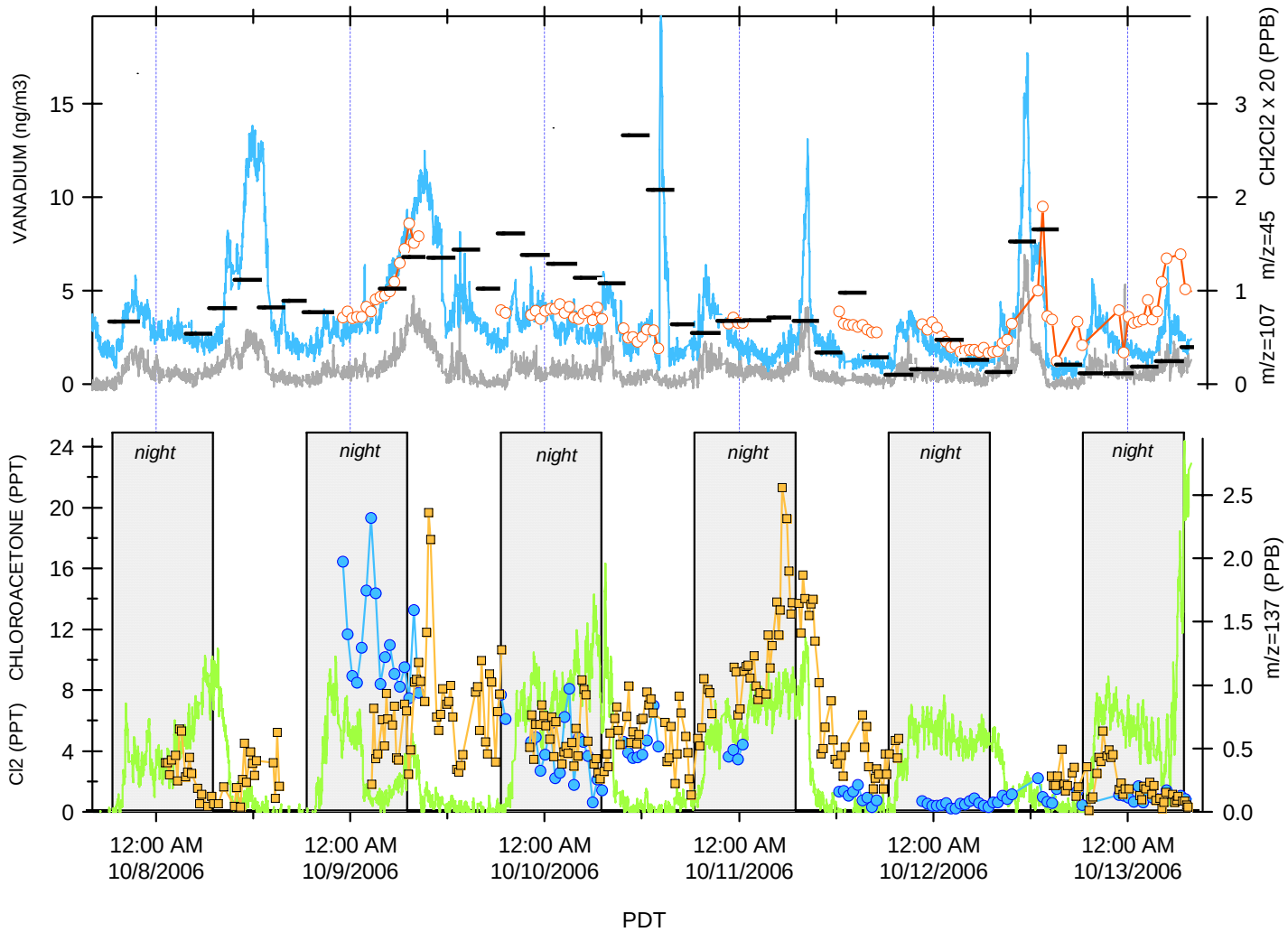

Figure 5.3.1 Time series of selected tracers during a period of elevated Cl_2. Upper panel: particulate vanadium levels are given by horizontal bars, bar length shows sampling duration; CH_2Cl_2 mixing ratios (open circles) are multiplied by 20 to better display data; grey and blue traces are PTR-MS measurements of C_2-alkylbenzene isomers (m/z = 107) and acetaldehyde (m/z = 45) respectively. Lower panel: Cl_2 (orange squares); chloroacetone (blue circles); and total monoterpenes (m/z = 137, green trace). Bottom panel shows nighttime periods defined by sunrise and sunset times.

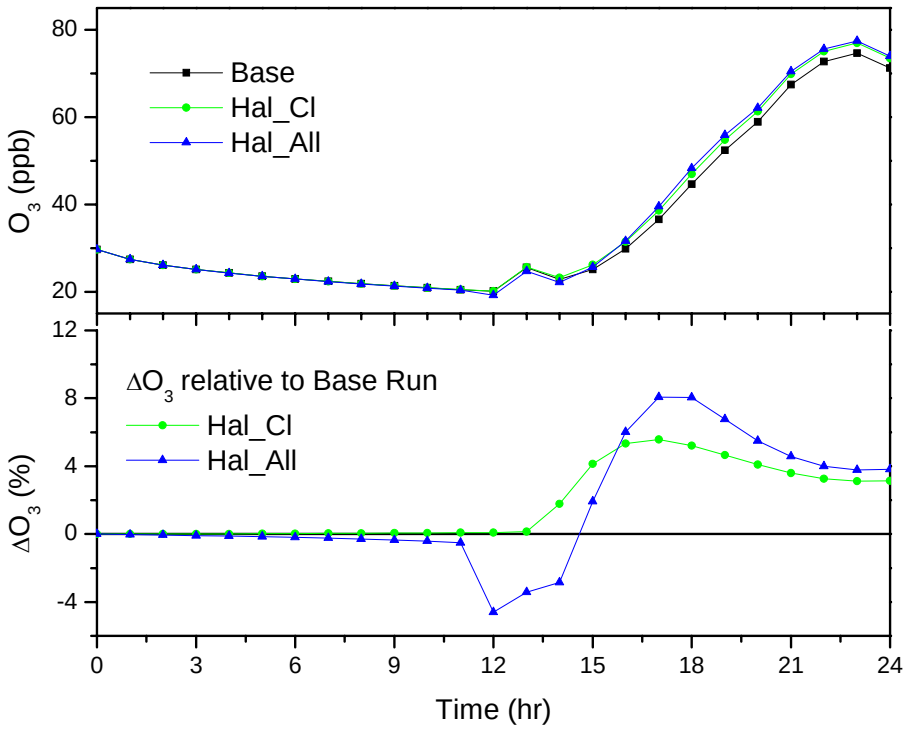

Figure 5.4.1 Modeled ozone mixing ratios for the three scenarios described in Table 5.2. The bottom panel shows the change in ozone in the presence of active halogen chemistry compared to the base run without halogens.

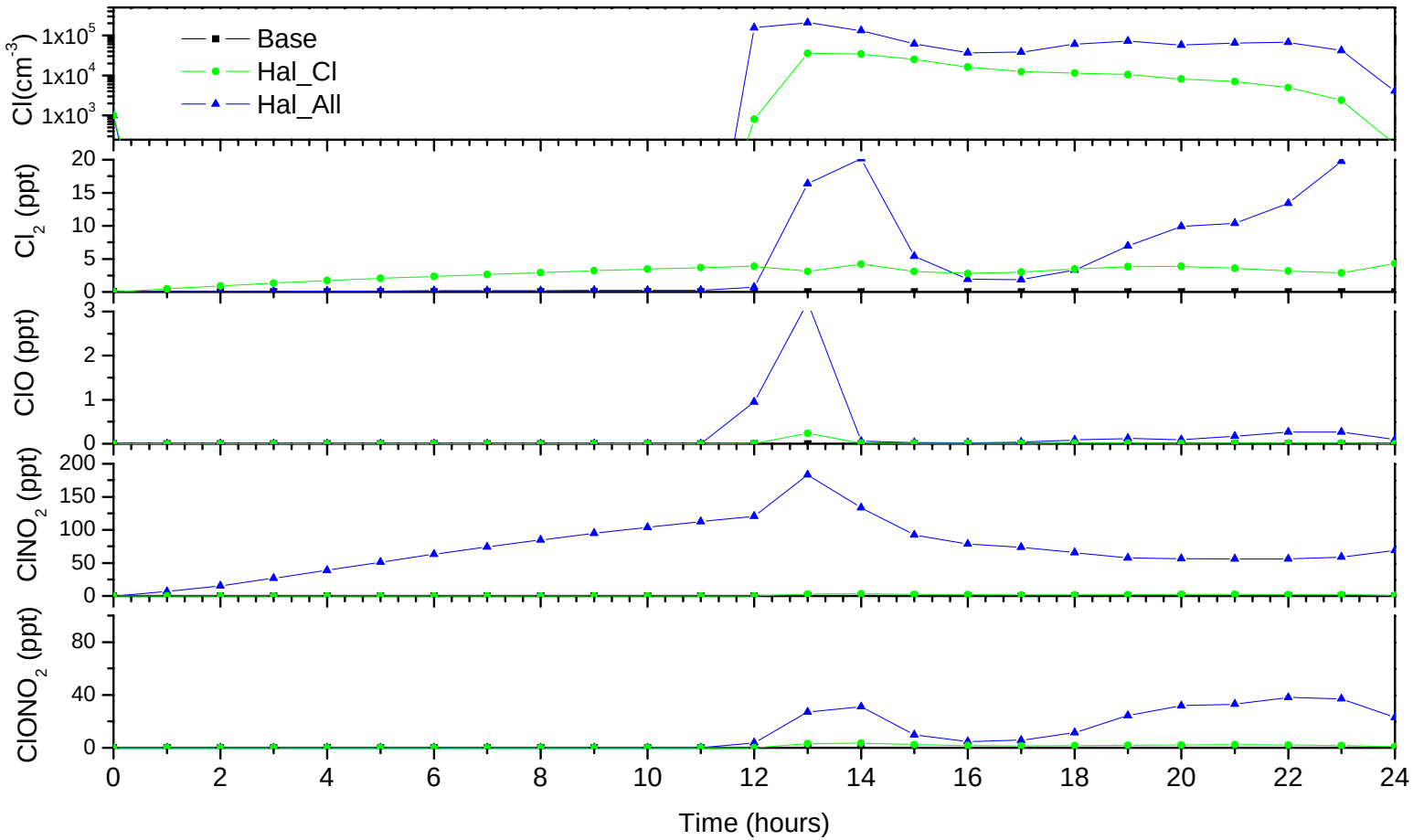

Figure 5.4.2 Modeled concentrations of the most important chlorine species for the scenarios described in Table 5.2.

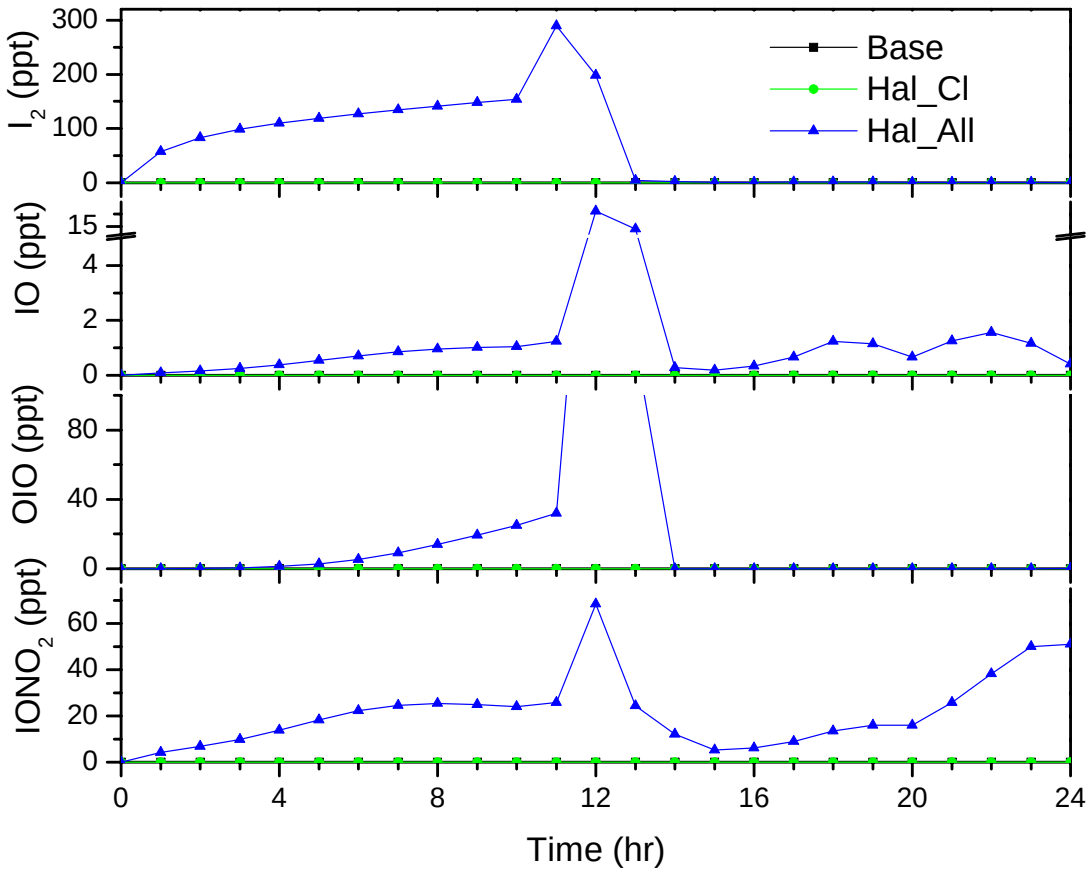

Figure 5.4.3 Modeled concentrations of the most important iodine species for the scenarios described in Table 5.2.

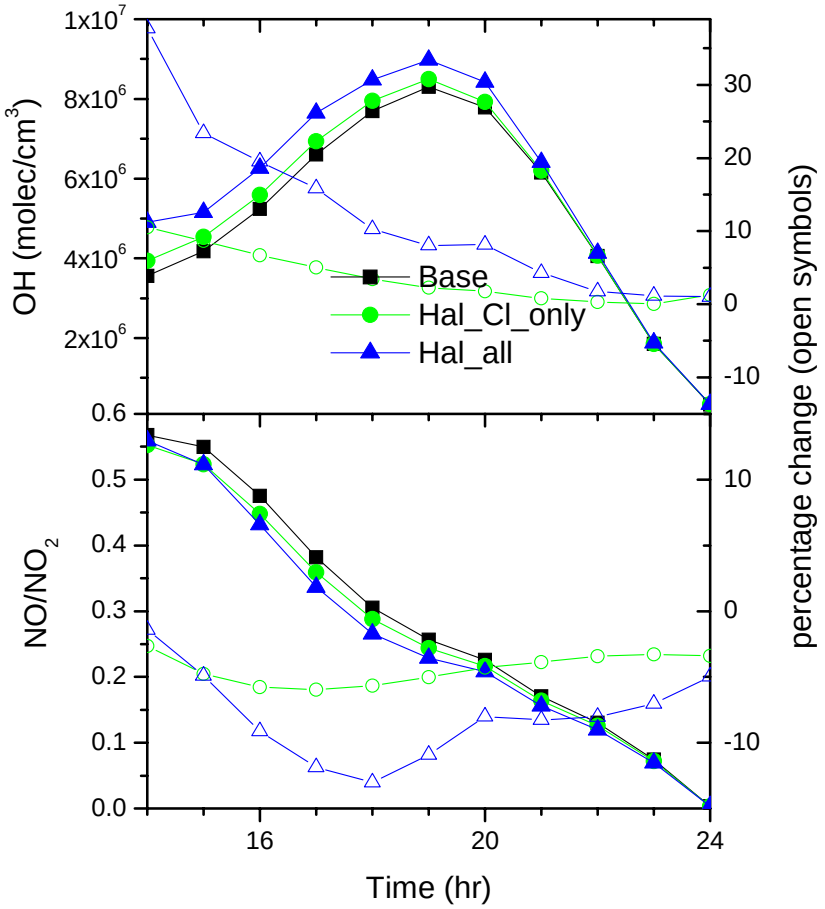

Figure 5.4.4 Modeled OH concentration and NO/NO_2 ratios for the modeled cases (closed symbols) and the percentage change for the two halogen cases compared to the base case without halogens (open symbols).